

UNCLASSIFIED

407 825

AD

DEFENSE DOCUMENTATION CENTER

FOR

SCIENTIFIC AND TECHNICAL INFORMATION

CAMERON STATION, ALEXANDRIA, VIRGINIA



UNCLASSIFIED

NOTICE: When government or other drawings, specifications or other data are used for any purpose other than in connection with a definitely related government procurement operation, the U. S. Government thereby incurs no responsibility, nor any obligation whatsoever; and the fact that the Government may have formulated, furnished, or in any way supplied the said drawings, specifications, or other data is not to be regarded by implication or otherwise as in any manner licensing the holder or any other person or corporation, or conveying any rights or permission to manufacture, use or sell any patented invention that may in any way be related thereto.

63-4-2

407 825

407 825

CATALOGED BY DDC

MEMORANDUM

RM-2553-PR

MAY 1963

AS AD NO.

THEORETICAL ANALYSIS OF
NEAR-FREE-MOLECULE HYPERSONIC FLOW
AT THE SHARP LEADING EDGE OF
A FLAT PLATE

A. F. Charwat

PREPARED FOR:
UNITED STATES AIR FORCE PROJECT RAND

RECEIVED
MAY 15 1963
7034 0

The RAND Corporation
SANTA MONICA • CALIFORNIA

MEMORANDUM

RM-2553-PR

MAY 1963

THEORETICAL ANALYSIS OF
NEAR-FREE-MOLECULE HYPERSONIC FLOW
AT THE SHARP LEADING EDGE OF
A FLAT PLATE

A. F. Charwat

This research is sponsored by the United States Air Force under Project RAND—contract No. AF 49(638)-700 monitored by the Directorate of Development Planning, Deputy Chief of Staff, Research and Development, Hq USAF. Views or conclusions contained in this Memorandum should not be interpreted as representing the official opinion or policy of the United States Air Force.

The RAND Corporation

1700 MAIN ST • SANTA MONICA • CALIFORNIA

PREFACE

Recent studies in the application of lifting surfaces and pointed slender cones to both glide vehicles and advanced re-entry vehicles have focused attention upon the aerodynamic performance of such configurations in sustained hypersonic flight through the lower ionosphere. In addition, interest has been exhibited by aerodynamicists and heat-transfer engineers in the fluid-mechanical and thermal phenomena which occur in the leading-edge region of a sharp wing which is in hypersonic flight at even lower altitudes.

This Memorandum examines a theoretical problem which is highly relevant to both of these applications: the analysis of the low-density hypersonic flow near the leading edge of a sharp flat plate. The analysis should be applicable to the determination of the incipient effects of intermolecular collisions upon the flow of a rarefied gas in the transition regime.

SUMMARY

The initial interactions between a hypersonic free stream and molecules emitted (reflected diffusely) by a cold flat plate immediately downstream of its sharp leading edge are analyzed by near-free-molecule theory. The results give the variations of the pressure, shear, and heat transfer at the wall. These are found to increase downstream from the leading edge and reach a maximum plateau, and a subsequent decay of the wall-transfer properties to continuum boundary-layer values can be inferred. The magnitude and location of this plateau compare well with available viscous pressure interaction data. An indication of the initial growth rate of the disturbed merged layer is also obtained from the analysis. It is found that this region is wedgelike and has a slope of approximately 45 deg for all hypersonic Mach numbers and for wall-to-free-stream-temperature ratios of the order of unity.

ACKNOWLEDGMENTS

The author is grateful for the many helpful discussions and the interest in this work expressed by T. Y. Li, P. S. Lykoudis, H. T. Nagamatsu, and Carl Gazley, Jr., of The RAND Corporation, and for the help received from Dr. Eugene Levin, now affiliated with Aerospace Corporation, in handling the often exasperating integrals.

CONTENTS

PREFACE	iii
SUMMARY	v
ACKNOWLEDGMENTS	vii
SYMBOLS	xi
Section	
I. INTRODUCTION	1
II. ANALYSIS	7
The Relative Mean Free Path	7
The Emission from the Surface	11
The Distribution of Free-Stream Molecules	15
Space Distribution of First-Scattered Molecules (Model V)	18
Discussion	23
III. THE INDUCED PRESSURE	29
Discussion and Comparison with Data	32
Second Approximation to n_{en}	42
Surface Shear Near the Leading Edge	45
Heat Transfer, Slip, and Temperature Jump	47
IV. EMPIRICAL EXTENSION OF THE RESULTS	49
Appendix: EVALUATION OF CONSTANTS	55
REFERENCES	61

SYMBOLS

- A, B = numerical proportionality constants
- C, D = proportionality factors relating molecular model characteristics to flow parameters
- C_f, C_h = skin-friction coefficient and Stanton number
- E_i = exponential integral
- F = empirical constant (essentially the inverse thermal-accomodation coefficient)
- f = velocity-distribution function
- G_i = collision-density distribution (Eq. (7)) of molecular group i
- K = wall-to-free-stream temperature factor (Eq. (22))
- K_0 = Bessel function of the second kind
- L_i = mean free path of a molecular group i diffusing into the atmosphere
- l_{ij} = free path of a molecular group i diffusing into molecules j only
- M' = ratio of mean free-stream velocity relative to the plate to the average (directed) thermal velocity in the free stream (Eq. (24))
- M_0 = Mach number, ratio of mean relative velocity to the speed of sound in the free stream
- n = flux of molecules per unit area (molecules/sec, unit area)
- P = surface pressure
- Re = Reynolds number based on free-stream conditions
- S = mutual collision cross section
- T = temperature (deg abs)
- V = magnitude of the vector velocity
- v, u = cross-stream and streamwise velocity components

- \bar{v}_T = free-stream mean (directed) thermal agitation
- x, y = streamwise and cross-stream coordinates (origin at leading edge)
- α, β = nondimensional coordinates x/L_e and y/L_e
- Γ_θ = normalization factor (Eq. (5))
- γ = scattering angles for primary encounters
- Θ = collision rate per unit volume
- θ, ξ = polar coordinates of a point (θ measured relative to the normal to the plate)
- $\bar{\theta}$ = normal momentum coefficient
- λ = Maxwellian mean free path in the free stream
- ρ = molecular number density (molecules/unit volume)
- Φ, Ψ = functions describing wall emission
- χ = hypersonic interaction parameter $M^3 \sqrt{Re}$

SUBSCRIPTS

- e = molecules emitted (reflected) from the surface
- en = molecules resulting from collisions of molecule e with n , and so on
- FM = free-molecule (collisionless) flow
- i, j = generic subscripts denoting classes of molecules
- i = incident molecules
- n = free-stream molecules
- p = surface of the plate
- s = free-stream stagnation conditions
- ∞ = free-stream static conditions
- \bar{x} = indicates averaging over the distribution of x

I. INTRODUCTION

Recent measurements^(1,2,3) of the surface pressure on flat plates in hypersonic flow at low densities have shown that there exists a measurable length downstream of the leading edge over which the concepts of first-order boundary-layer interaction theory do not apply. There is evidence of a pressure plateau, the magnitude of which depends both on the Mach number and also, apparently, on the temperature of the flow relative to the wall temperature. Downstream of this plateau the pressure decays at a rate which is in qualitative agreement with boundary-layer interaction concepts but which does not agree with currently available first-order theories. Upstream of it the pressure must rise, a phenomenon which is entirely outside of the scope of the continuum-flow analytical model. Schlieren photographs⁽¹⁾ show this initial growth of the disturbed region and suggest an exponential shape for it. It is interesting to note that this structure of the flow is independent of the density, provided only that the leading edge is sufficiently sharp to prevent the formation of a bow wave. The flow passes through all regimes of aerodynamics, from free-molecule to continuum, in a certain distance downstream from the leading edge.

In this Memorandum, the origin of the flow over a semi-infinite plate which has a sharp leading edge aligned with the stream is investigated by a kinetic-interaction technique. The model is illustrated schematically in Fig. 1. The incident molecules, which belong to a molecular group defined by the characteristics of their mean

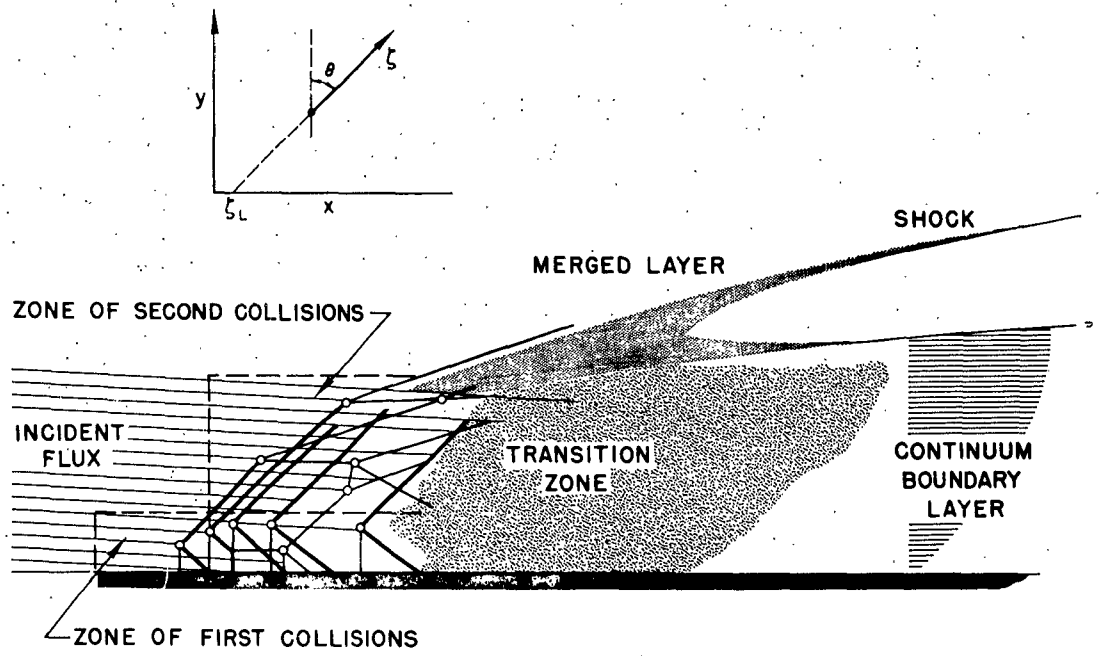


Fig. 1—Sketch of initial interactions

motion, approach the plate nearly tangentially. (The analysis is restricted to high Mach numbers.) Another group, particles emitted by the wall, diffuse into this atmosphere at right angles to the free stream. These particles collide; this collision knocks them out of their groups and replaces them by particles of a new group, the characteristics of which can be derived from the dynamics of the encounter. The paths of these first-scattered molecules are shown on Fig. 1 by the darker lines; the figure, and the analysis as well, is restricted to the case in which the mean velocity of the emitted particles is low compared to that of the incident ones, relative to a coordinate system fixed to the plate.

The spatial distribution of the first collisions (zone of first collisions) is calculated. It is characterized by the convective distance between collisions, a relative mean free path of one group diffusing into the atmosphere of the other group--not by the mean free path of either group by itself. Obviously, if the mean velocities of each group are different, the zone of first collisions will be geometrically distorted.

By knowing thus the source distribution of the first-scattered molecules, their paths can be calculated and their decay due to second collisions or their capture by the surface can be found. The scale of the zone of second collisions is characterized again by a relative mean free path of the scattered molecules in the atmosphere of the others; this mean free path is different from that of the first collisions. An examination of the total normal momentum due to molecules of the various groups captured by the surface yields the

local surface pressure, which is the primary result of this analysis.

The analysis of this interdiffusion and scattering of successive groups of molecules, assuming a one-sided emitting-collecting surface, can by the present technique be continued past the first-scattered group as long as distinct characteristic interaction parameters for each group (mean free paths) can be defined. This turns out to be practical when there are only a few families in a given region in space and when the differences in their characteristics are large. In other words, the analysis is practical in the zone of initial collisions (up to the third) when the flow is hypersonic (nearly Newtonian) and when the wall temperature (the mean velocity of the emission by the wall) is low compared to the free-stream stagnation temperature. Nonetheless, significant results are obtained because the very first interaction between a free-stream molecule and one emitted by a surface brings about a violent change in the contribution of the former molecule to the normal momentum transfer to the surface: The collision scatters them at an average of 45 deg to the relative direction of impact. Thus it transforms one-half the free-stream momentum per molecule into normal momentum directed at the surface (cold surface).

Downstream of the initial collision zone one distinguishes a transition zone in which further collisions bring about the final establishment of an equilibrium shear layer. In an equilibrium shear layer, the transverse momentum transfer from the free stream to the wall proceeds by a collision-diffusion process rather than by direct molecular convection. The present analysis cannot be carried out

formally into the transition zone, although some of its characteristics, based on the indications of the first-collision calculation, are presented in the text. Figure 1 shows schematically the structure of the leading-edge zone to the formation of a continuum boundary layer as it is visualized in this discussion.

Similar initial-collision calculations performed for blunt-body flows^(4,5) have shown that in spite of their restrictions, the theory yields a physically meaningful picture of the phenomena and leads to the definition of important interaction criteria and similarity parameters. This is the principal purpose of the present analysis. We view it as a subtle form of dimensional analysis rather than as a quantitative theory. We hope to obtain from it a qualitative framework useful, perhaps, for constructing a semiempirical correlation of the data, which at present escapes generalization. (Note the wide scatter of the experimental measurements when plotted against the continuum interaction parameter.) Accordingly, we make several simplifying assumptions in the calculations, provided that they do not distort the essential physical phenomenon. An accurate solution of the leading-edge problem will have to be attempted along different lines, perhaps by use of a moment method of solving the Boltzmann equations.⁽⁶⁾ An important feature of the analysis will be its ability to span the entire transition from free-molecule to continuum flow.

It is perhaps worth mentioning in this discussion the difference between the present technique and other methods which have also been called first-collision analyses--for instance, the method proposed

by Willis.^(7,8) They are not equivalent. Willis finds a first-order correction to the free-stream distribution function by iterating on a simplified (Krooks' model) Boltzmann integral, starting with the same two Maxwellian groups of molecules, free-stream molecules and those emitted by the wall. This technique differs from the present method in that the mean-free-path characteristic of the interaction is not a priori a constant. The present iteration (not in a mathematical sense) on successive groups of scattered molecules, although numerically more approximate, avoids the need for computer techniques and yields a clearer physical picture of the field of the interactions than does Willis' method.

II. ANALYSIS

THE RELATIVE MEAN FREE PATH

In order to describe the interdiffusion of the molecular groups we consider the length of flight of a particle of the group i in an atmosphere of particles j

$$l_{ij} = \frac{V_i}{\Theta_{ij}} = \frac{V_i}{\rho_j S_{ij} |\underline{V}_i + \underline{V}_j|} \quad (1)$$

where Θ_{ij} is the collision rate of i with j , S_{ij} is the mutual collision cross section, and $|\underline{V}_i + \underline{V}_j|$ is the magnitude of the relative (vector) precollision velocity.

In general, the factors in Eq. (1) are functions of both velocity and physical spaces. A mean free path can be obtained, in principle, by carrying out the appropriate integrations. In particular, the local decay of beam i by collisions with j is

$$dn_i = \int_V \int_\Theta \int_\zeta \frac{\rho_j S_{ij} |\underline{V}_i + \underline{V}_j|}{V_i} n_i f_i e^{-\int_k \frac{1}{\sum \ell_{ik}} d\zeta} dV d\Theta d\zeta \quad (2)$$

where f_i is the distribution function of molecules i emitted from a point in the polar direction θ at velocity V_i , and where the integration is performed over all velocity and physical spaces (polar coordinates θ, ζ).

Equation (2) leads to a difficult implicit problem unless the product $\rho_j |\underline{V}_i + \underline{V}_j|$ is constant or prespecified in geometric space. If j is to represent a particular group (for instance, the free-stream

molecules), then such an assumption restricts the validity of the calculation to the extreme near-free-molecule zone and cannot correctly reproduce the interesting feature of the leading-edge problem.* However, we can consider j as representing all the groups in the zone of collisions with the groups i . This assumption requires that the magnitude of the relative precollision velocity vector be adequately represented by an average of all the possible collisions. Now, we shall concern ourselves only with the initial collisions which follow an encounter between a molecule emitted (reflected) from the wall (type e) and a free-stream molecule (type n). We shall also assume $V_e \ll V_n$, that is, that the wall emission is cold in comparison with the stagnation temperature of the flow. In this case the relative vector velocity for the most probable spherically elastic first collision is simply V_n , for all possible second collisions $(1/\sqrt{2})V_n$, and for nearly all third collisions $1/2 V_n$ (see Fig. 2).** Only about 7 per cent of the quaternary molecules begin to have an upstream velocity component.

It follows, provided that there exist relatively well-defined space domains populated only by molecular groups which have collided not more than three times, that

$$\rho_j \frac{V_i + V_j}{|V_i + V_j|} = \rho_j \frac{|V_i + V_j|}{|V_i + V_j|} = \text{Const for the group} \quad (3)$$

is physically significant. It turns out that such domains exist as

*This assumption is implied in previous analyses of blunt-body flow.^(4,5)

**See, for instance, Kennard, Kinetic Theory of Gases, Chapter 3 (McGraw). The vector diagrams are based on momentum conservation for a two-dimensional gas.

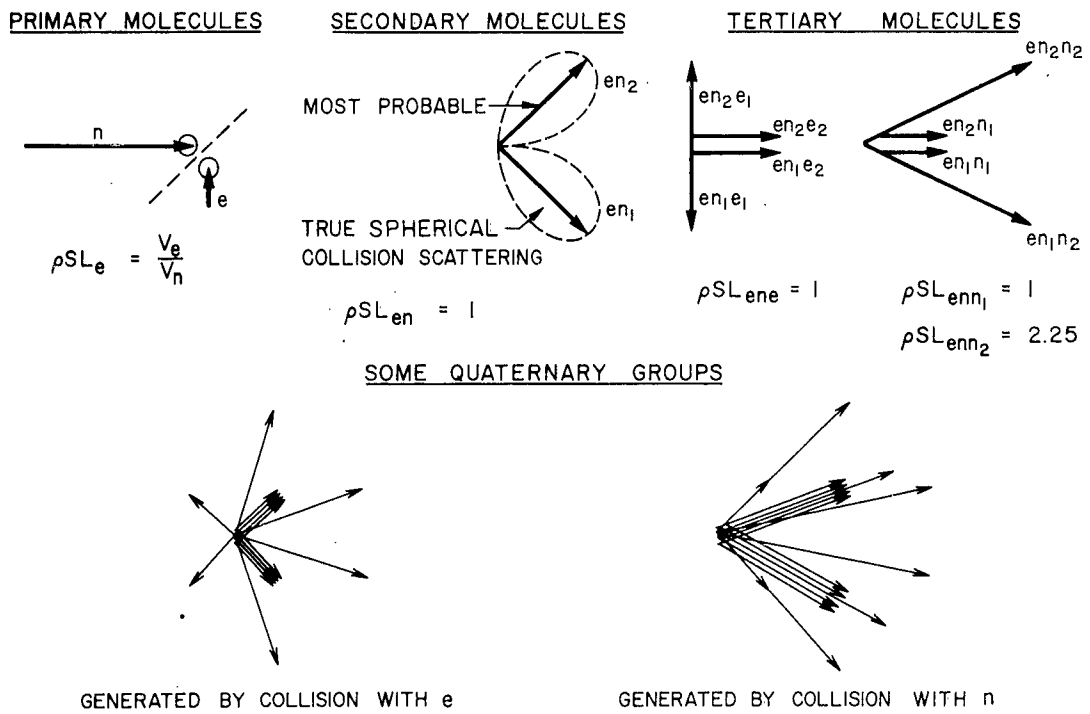


Fig. 2 — Most probable scatterings in successive collisions

long as the molecular motion is predominately unidirectional in the initial-collision zone at the leading edge for hypersonic flow over a cold surface.

The foregoing is a fundamental restriction on the validity of the present near-free-molecule technique. The other assumptions which are made in this calculation and which are outlined below are not essential and can be removed if desired. Their only purpose is to permit a closed-form solution.

The individual particle velocity V_i of a group i is replaced by an average \overline{V}_i over velocity space. Note that the dependence of V_i on velocity always feeds back through the intermediary of particle-particle collisions to the description of the distribution in velocity space of the fundamental group of molecules e emitted by the wall in a given polar direction θ , about which nothing is known. Conversely, the distribution of the average velocity in the polar directions θ from the collision center can be conserved without added difficulty by writing

$$\overline{V}_i = \overline{V}_i^\theta \Psi(\theta)$$

For example, in the case of Lambert diffuse emission from a Maxwellian oven into a half-space, we have

$$\Psi(\theta) = \cos \theta, \quad -\frac{\pi}{2} < \theta < +\frac{\pi}{2}$$

as usual. Since V_i is not a function of ζ , the beam-decay formula, Eq. (2), reduces to the simple form

$$\left(\frac{dn_i}{n_i}\right)_{(\theta)} = \frac{1}{L_i \bar{V}(\theta)} e^{-\frac{\zeta}{L_i \bar{V}(\theta)}} d\zeta \quad (4)$$

which upon integration through the polar space θ from the source reduces to the classical form applicable to a homogeneous molecular field; L_i^* is here a constant mean length characterizing the collisions of that group with all other molecules.

We shall also assume in the calculations that the motion of all molecules is restricted to two dimensions in a plane parallel to the mean flow and perpendicular to the leading edge. It is clear that in the application to a two-dimensional problem (infinite span) this assumption does not change the pattern of the interactions at all and affects the numerical constants only slightly.

THE EMISSION FROM THE SURFACE

Let $\phi_{(e)}$ be the polar density distribution of the n_e molecules per unit surface and time emitted by an element dx_p of the plate at x_p into a wedge $\pm \Delta \theta$ about θ . By using Eq. (4), the density of their collisions in space (collisions per unit time, per element of volume $2\Delta\theta d\zeta$) is

$$n_e \frac{\Gamma(\theta)}{\bar{V}(\theta)} \frac{e^{-\frac{\zeta}{L_e \bar{V}(\theta)}}}{L_e \zeta} \quad (5)$$

where $\Gamma(\theta)$ is a normalization factor

*A refinement worth noting is this: The proper value of V_i which enters Eq. (4) in the exponent is not numerically identical to the "mean" velocity in the sense of temperature of that molecular group.

$$\Gamma(\theta) = \frac{1}{2\Delta\theta} \frac{\int_{\theta - \Delta\theta}^{\theta + \Delta\theta} \phi(\theta) d\theta}{\int_{-\frac{\pi}{2}}^{+\frac{\pi}{2}} \phi(\theta) d\theta} \quad (6)$$

In order to obtain the total number of collisions per unit volume and time at a generic point in the half-space above the plate it is necessary to integrate along the emitting surface. Thus

$$G_e = \int_0^{x_p} n_e \frac{\Gamma(\theta)}{\Psi(\theta)} \frac{e}{L_e \zeta} dx_p \quad (7)$$

where the coordinates ζ and θ (θ measured from the perpendicular to the plate) relate a point in space to the source of emission, and where $n_e = n_e(x)$ is generally a function of position along the surface as dictated by a mass balance among the emitted and all the intercepted molecules at x_p . It may include a mass source, such as sublimation of the plate material. Clearly, this depends implicitly on the results of the analysis, and it is necessary to accept either an approximate or an iterative procedure to continue. A relatively simple scheme is to expand n_e in series in x_p with coefficients to be determined later from auxiliary mass-conservation conditions. However, it was found that although this is conceptually simple, it complicates the subsequent integrals sufficiently to demand a numerical solution.

The functions ϕ (which is equivalent to Γ) and Ψ describe the

geometric character of wall emission. Since very little is known about this character, we must make some assumptions in order to facilitate the integration. Some typical models considered are shown in Fig. 3. These models include the classical Lambert Law (Model I), a density distribution of a specular type based on indications of the recent experimental⁽⁹⁾ and theoretical⁽¹⁰⁾ studies, and the simplest possible model of a beam-like monochromatic emission from the wall, of an arbitrary degree of specularity described by $\bar{\theta}$ (Model V).

Equations (8), (9), and (10) below show the G-integrals (Eq. (7)) for three of the models. The result for Model I is approximate and is obtained by replacing the exponential e^{-x^2} by a factor $\frac{1}{(1+x^2)}$ which behaves similarly to it. Using only a constant term in the expansion for n_e^*

Model I

$$\frac{G_e L_e}{n_e} = \frac{1}{4\sqrt{1+\beta}} \ln \frac{\alpha - \sqrt{1+\beta}\sqrt{\alpha^2 + \beta^2}}{\alpha + \sqrt{1+\beta}\sqrt{\alpha^2 + \beta^2}} + \frac{1}{4} e^{-\frac{1}{2}\beta} K_0\left(\frac{1}{2}\beta\right) \quad (8)$$

Model II

$$\frac{G_e L_e}{n_e} = \text{Ei} \left[-\frac{\alpha^2 + \beta^2}{\beta} \right] - \text{Ei} [-\beta] \quad (9)$$

Model V

$$\frac{G_e L_e}{n_e} = e^{-\frac{\beta}{\cos \bar{\theta}}} \quad (10)$$

Figure 4 shows lines of constant parameter ($G_e L_e / n_e$) in the

* K_0 is the Bessel function of the second kind and Ei is the exponential integral.

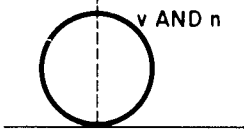
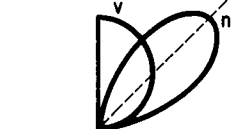
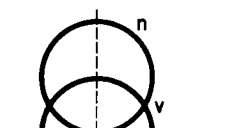
MODEL	SCHEMATIC	DISTRIBUTIONS	
I		$\psi = \cos \theta$ $\Theta = \cos \theta$	LAMBERT LAW
II		$\psi = \cos \theta$ $\Theta = \sin 2\theta$	COSINE VELOCITY, SPECULAR
III		$\psi = 1$ $\Theta = \cos \theta$	UNIFORM VELOCITY, DIFFUSE
IV		$\psi = 1$ $\Theta = \sin 2\theta$	UNIFORM VELOCITY, SPECULAR
V		$\psi = 1$ $\Theta = 1$	MONOCHROMATIC BEAM AT $\bar{\theta}$

Fig. 3—Wall-emission models

initial-interaction zone for Models I and II. Model V fails to reproduce the two-dimensional nature of the leading-edge zone and the upstream propagation of the disturbance seen in Fig. 4. However, the extent of this zone is of the order L_e , and it will be shown later that the length characterizing the molecular exchanges with the surface (induced pressure) is of the order $L_e M$. Therefore, when the Mach number is sufficiently high, the stand-off distance of the interaction zone relative to the leading edge and the influence of the type of the wall emission become unimportant.

Note that Eqs. (8) and (9) already imply the assumption of a constant (streamwise) surface-emission density. However, the G_e function for Model V, Eq. (10), permits this x-dependence to be carried on. This may offer advantages in further studies, such as the inclusion of mass addition, which outweigh the shortcomings of this simple distribution.

THE DISTRIBUTION OF FREE-STREAM MOLECULES

The space density of the incident molecules diminishes as they penetrate the interaction zone because of collisions which knock them out of their class. Two molecules of another class per collision, the characteristics of which can easily be obtained from the collision dynamics, are generated in their place. The rate of disappearance of incident molecules, n , due to collisions with the wall-emitted ones, e , is, per unit volume and unit time

$$\frac{\rho_n}{\rho} G_e \quad (11)$$

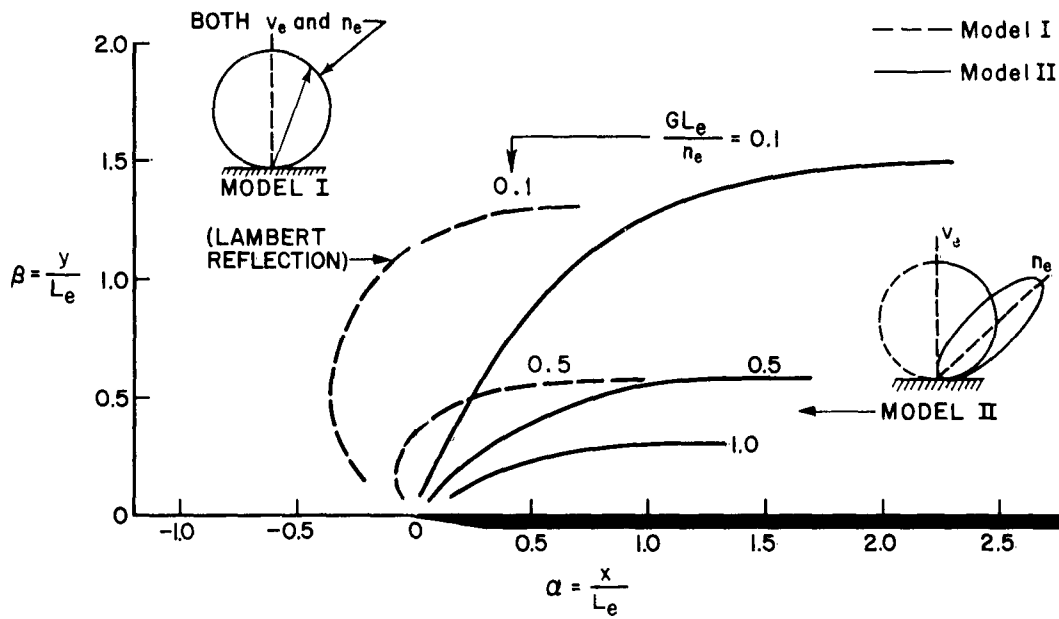


Fig. 4—Lines of constant density of first collisions G ($\frac{\text{collisions}}{\text{vol. time}}$) for diffuse- and specular-emission models

which is also twice the number of e_n , the first-scattered molecules, generated per unit volume and time at that point. Since the motion of e_n is known, it is conceptually possible to calculate G_{en} in space and the rate of disappearance of n by collisions with e_n , and so on. The local density of the n molecules in space is given by the solution of the conservation equation

$$u_n \frac{\partial \rho_n}{\partial x} + v_n \frac{\partial \rho_n}{\partial y} = - \frac{\rho_n}{\rho} \sum_j G_{nj} \quad (12)$$

In this general form the problem is extremely complicated. We shall consider in what follows only the first iteration; that is, we shall disregard all but the first collision. This can be interpreted physically by stating that we are not distinguishing between the two tertiary molecules (for example enn and ene) and the two molecules which generated them. From the standpoint of the cross-stream-momentum flux, which is the principal result of this analysis, this is correct because downward-directed momentum is generally conserved in such collisions. From the standpoint of the space distribution of these molecules, the approximation is acceptable because the most probable vector paths of the enn or the ene molecules do not differ too much from those of the generating ones; also, their speeds and their mean free path in the gas are not greatly different.

If the flight Mach number is sufficiently high, the cross-stream-diffusion term (pseudo-Newtonian flow) can be neglected.* Then the

*A better but more complicated solution can also be obtained if the second term in Eq. (12) is replaced by a self-diffusion term $\lambda \partial^2 \rho_n / \partial y^2$. It is interesting to note that the result then depends also on the free-stream mean free path λ .

local density of the incident molecules in the interaction zone is simply

$$\rho_n(x,y) = \rho e^{-\int_{-\infty}^x \frac{G_e}{\rho V_n} dx} \quad (13)$$

The restriction to hypersonic flows is consistent with previously discussed assumptions concerning the existence of a characteristic interaction distance, L_e . The density, ρ , in the exponent of Eq. (13) is the total local density (all groups), and the product ρV_n is constant (see Eq. (3)) ($V_e \ll V_n$).

The exponent $H = \int G_e dx$ in Eq. (13) can be obtained in the form of sums of integral functions for all the models considered. The results are, however, too complicated for further closed-form analysis except in the case of Model V. In that case, from Eq. (10)

$$\ln \frac{\rho_n}{\rho} = - \left(\alpha - \beta \tan \bar{\theta} \right) \left(\frac{n_e}{\rho V_n} \right) e^{-\frac{\beta}{\cos \bar{\theta}}} \quad (14)$$

Here $\bar{\theta}$ is the angle of the beam inclination.

SPACE DISTRIBUTION OF FIRST-SCATTERED MOLECULES (MODEL V)

Each $(\rho_n/\rho G_e)$ collision per unit volume and time produces two en molecules at that point in space. Their motion relative to the collision center can be specified in terms of the motions of the colliding pair without difficulty but at the cost of considerable algebraic complexity. The problem can be simplified without essential physical error by considering only the most probable collision, in which case the two en molecules are emitted in monochromatic

beams from the collision center along two distinct angles, γ_1 and γ_2 . In particular, in the extreme case when V_e is zero (stationary scatterer), $\gamma_1 = \gamma_2 = \pi/4$, the vector velocity of both en molecules is $(1/\sqrt{2})V_n$, and the velocity components normal and tangential to the flow of each molecule are $(1/2)V_n$.

However, a better relation for the properties of the scattered molecules, which maintains at least approximately their dependence on the emission velocity, is

$$V_{en} = \frac{1}{\sqrt{2}} V_n \left(1 \pm \frac{V_e}{V_n} \right) \quad (15)$$

$$V_{en} = \frac{1}{2} V_n \left(1 \pm \frac{V_e}{V_n} \right) \quad (16)$$

$$\gamma = \pm \frac{\pi}{4}$$

The positive and negative signs refer to the upward and the downward family, respectively.

The concern with this new group of molecules brings forth a new characteristic mean free path. From the basic definition

$$L_{en} = \frac{V_{en}}{\rho S_{en} |\vec{V}_{en} + \vec{V}_j|} \sim \frac{1}{\rho S_{en}} \sim \lambda \quad (17)$$

where the second equality is obtained from the most-probable-collision diagram and Eq. (16). It is notable that the mean free path of scattered molecules equals the Maxwellian mean free path in the free stream.

It is identical for both the en-o and the en-e encounters (j in Eq. (17) is n and e, respectively) in this particular case of the cold wall. Thus this single characteristic length adequately describes the

interactions in the domain of the first-scattered molecules.

Let us consider separately the two scattered beams. We consider first the upward flux in order to outline approximately the character of the interaction zone.

Upward Flux

The balance of en molecules along their path ζ is

$$(\rho_{en})_{\zeta} = \int_{\zeta_L}^{\zeta} (\rho_{en})_{\zeta_0} e^{-\frac{\zeta - \zeta_0}{L_{en}}} d\zeta_0 \quad (18)$$

where the first factor in the integral represents the local source density of en molecules at a generic point, ζ_0 , and the exponentials describe their decay along their path, which is assumed to be characterized adequately by a single mean free path, L_{en} . The integration is performed from an adequate lower limit (the plate surface), denoted by ζ_L . The source term is

$$(\rho_{en})_{\zeta_0} = \left(\frac{\rho_n}{\rho} G_e \right)_{\zeta_0} \quad (19)$$

where G_e represents all the collisions of molecules, e, at the point ζ_0 at which the fraction ρ_n/ρ generates the en molecules under consideration.

For the case $\bar{\theta} = 0$ and Model V one finds for $\alpha > \beta$

$$\frac{\rho_{en}}{\rho} = \frac{V_n}{V_{en}} \left(\frac{L_{en}/L_e}{1 - \frac{L_{en}}{L_e} \cos \gamma_1} \right) \left(\frac{1}{\alpha - \beta \tan \gamma_1} \right).$$

$$\cdot \left[\begin{array}{c} - \frac{\beta L_e}{L_{en} \cos \gamma_1} + \frac{n_e}{\rho V_n} (\alpha - \beta \tan \gamma_1) \\ - \beta \left(1 - \frac{L_e}{L_{en} \cos \gamma_1} \right) \\ - \left(\frac{n_e}{\rho V_n} \right) (\alpha - \beta \tan \gamma_1) \left(e^{-1} - 1 \right) \end{array} \right] \quad (20)$$

Using Eqs. (16) and (17), and also Eqs. (24) and (25), which relate $n_e/\rho V_n$ and V_e/V_n to the two fundamental parameters of the flow, one finds

$$\frac{\rho_{en}}{\rho} = \frac{1}{M'} \left(\sqrt{2} + \frac{K}{M'} \right) \left(1 - \frac{K}{M'} \right) \cdot \left[\frac{\alpha}{M'} - \frac{\beta}{M'} \right] e^{-\frac{M' - K}{M'}} - \frac{\alpha - \beta}{M'} \quad (21)$$

where K is related to the wall-to-free-stream temperature ratio

$$K = \sqrt{2} M' \frac{V_e}{V_n} \sim \sqrt{2} M' \sqrt{\frac{T_w}{T_s}} \sim \sqrt{\frac{T_w}{T_\infty}} \quad (22)$$

and M' is a molecular speed ratio defined by Eq. (24). This integral is approximated somewhat by neglecting an exponential factor in the integrand. Because of this, it is not valid in the neighborhood of $\alpha = \beta$. An expression similar to Eq. (21), and valid for $\alpha < \beta$, is also found but for the sake of brevity will not be shown.

Lines of constant density ratios of both the n and the en molecular groups (for two specific cases) are plotted in Fig. 3. This

can be compared with the schematic history of the molecular motion outlined in Fig. 1.

Downward Flux

The second family of the en molecules is directed toward the surface. Noting the relative magnitude of L_e , which measures the distance from the surface of the plate from which they originate, and L_{en} , which measures the length of their path, we conclude that in the cold-wall case the overwhelming majority of these en molecules will strike the surface. Moreover, the most probable secondary collisions (en-e or en-o) do not change the normal momentum intercepted by the surface. Only tertiary collisions ene-o, and so on, transform further a portion of the streamwise momentum into momentum normal to the plate. If the calculation is to be interrupted by this family of secondary molecules, then a better result for the total momentum interchange with the surface is obtained by neglecting the tertiary collisions entirely and assuming that all the en_2 molecules generated in the interaction zone reach the plate. The corresponding integral, analogous to Eq. (18), does not contain the exponential-decay factor. Carrying out the integration with the appropriate limits (over the quadrant above the plate) one finds to the same approximation the following expression for the flux (molecules/second-unit length) to the plate

$$\frac{n_{en}}{n_e} = \frac{M'}{\alpha} e^{-\frac{\alpha p}{M'}} \left[-1 + e^{-\frac{\alpha p}{M'} \left(e^{-\alpha \cot \lambda_2} - 1 \right)} \right] \quad (23)$$

This is shown in Fig. 4 for various Mach numbers (and $\gamma_2 = \pi/4$, as before).

DISCUSSION

The analysis has resulted in several characteristic parameters of interest. Since the number of scattered molecules, n_e , must be equal to the flux of molecules to the plate, and since in this approximation n_e was assumed to be constant and therefore equal to the free-stream cross-flow flux

$$n_e = \rho \bar{v}_T \therefore \frac{n_e}{\rho V_n} = \frac{\bar{v}_T}{V_n} \equiv \frac{1}{M'} \quad (24)$$

where \bar{v}_T is the average directional free-stream thermal agitation. Thus the first parameter which describes the density of the free-stream group involves a factor proportional to the reciprocal of the Mach number.

Using this in Eq. (14), it is seen that the decay of the free-stream molecules occurs in a rectangular region ($\beta = \alpha/M'$), which is equivalent to ($L_e \cdot ML_e$). It is stretched in the flight direction by M . As M goes to infinity (Newtonian flow), the whole interaction zone (the shock layer and the boundary layer) lies identically on the surface.

The well-known relations between the interaction length, L_e , and gasdynamic parameters is

$$L_e = \sqrt{2} \lambda \frac{V_e}{V_n} \sim \sqrt{2} \lambda \frac{1}{M'} \sqrt{\frac{T_w}{T_\infty}} \quad (25)$$

where λ is the mean free path in the free atmosphere, and T_w is the wall temperature. It follows that the physical distance from the leading edge, x , in which a fixed percentage (or all) the free-stream

molecules have collided is not a function of Mach number but of gas density and of the wall-to-free-stream temperature ratio T_w/T_∞ only. There is obviously a singularity for $T_w = 0$ which has no physical meaning.

The field of decay of the en group is more complex than that of the n group. It depends on the spatial density of e-n collisions and on the decay characteristics of the en group itself. The decay occurs in a streamwise length of the order of $L_e M$, which is the dimension of the first-collision zone generating the en molecules, and in a cross-stream distance zone which has thus the dimensions

$$\lambda \frac{T_w}{T_\infty} \cdot \lambda$$

It is approximately square and on the order of the free-stream mean free path. It is only slightly stretched streamwise with the square root of the wall-to-free-stream temperature ratio, and it is essentially independent of the Mach number (see also Fig. 5). This appears to be a fundamental characteristic of the initial growth of the disturbed layer over the plate. It has a slope of the order of unity rather than the slope of infinity which is implied by continuum boundary-layer theory. It does not seem to follow the exponential function suggested in Ref. 1.

The flux of secondary molecules to the plate increases from the leading edge to a maximum, as seen in Fig. 6. Beyond this point it decreases because the interaction zone is being depleted of the free-stream molecules, n, which generate the flux. It is of course incorrect to imply that the total mass and momentum flux to the surface decreases;

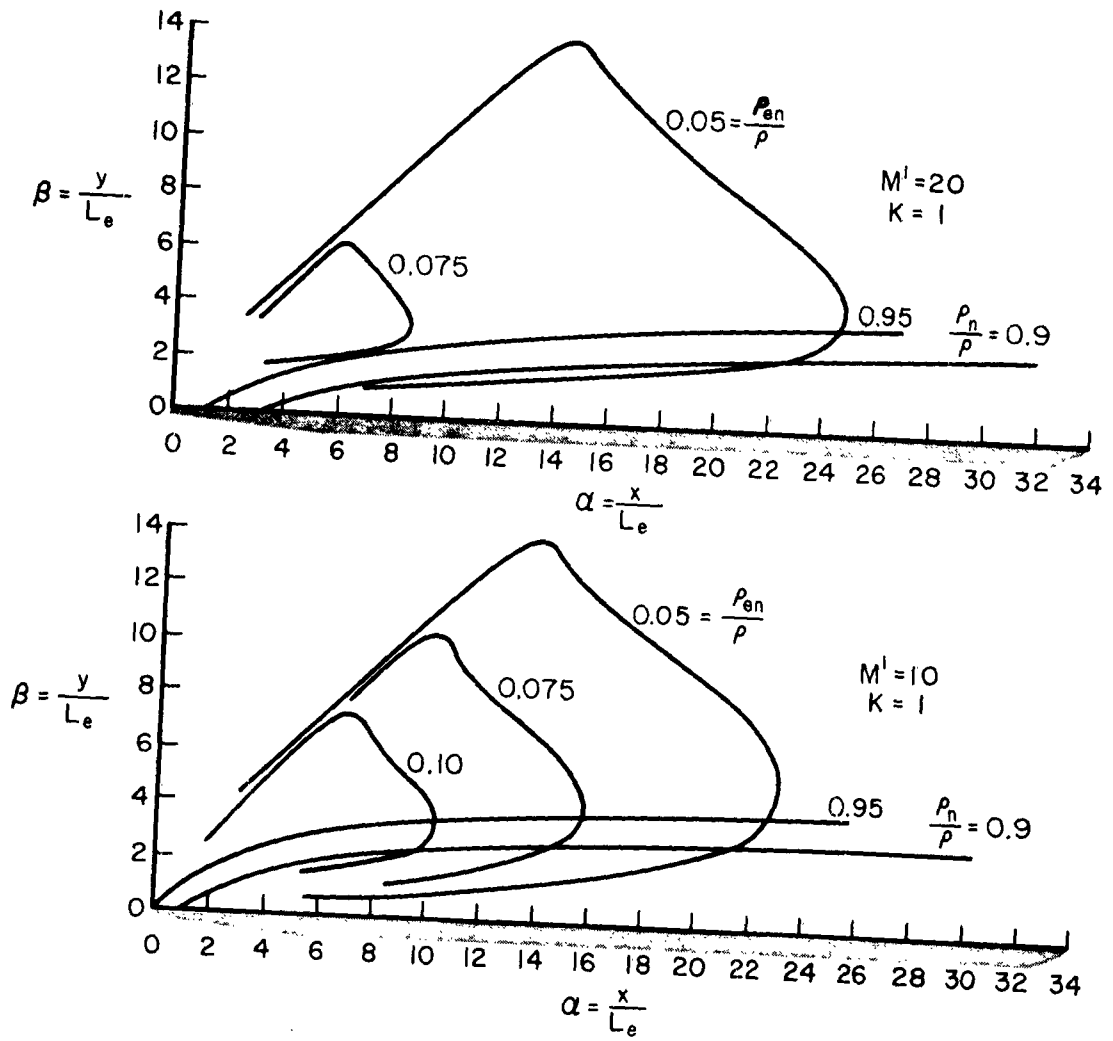


Fig. 5—Calculated local density of incident and scattered molecules

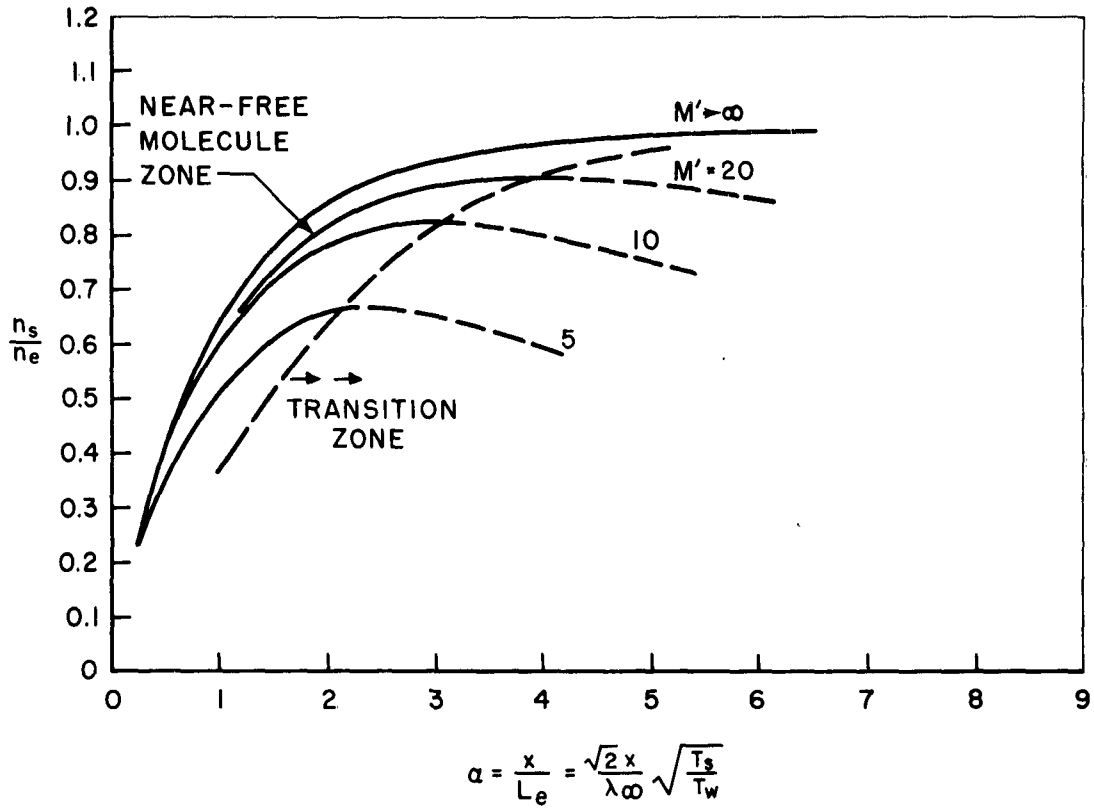


Fig.6 — Flux of scattered molecules to wall

tertiary and further molecules of all kinds make up the difference. We shall assume that the initial-collision zone is bounded on the downstream side by the locus of maxima of the flux of en molecules.

In this paper we wish to interrupt the "iteration" with the family of en molecules, yet we should like to sketch, at least approximately, the further development of the flow. Following the initial-collision zone is a transition zone in which the molecular families multiply in a geometric progression, and there are no definite space domains in which one family or a reasonably small number of families dominates. This can be seen from consideration of the simple vector diagrams of the successive collisions. Already one of the tertiary collisions (en-e) generates a molecule which moves upstream. Thus the directionality of the motion which makes this kinetic near-free-molecule analysis feasible is rapidly lost in the transition region, and more complete integral kinetic methods must be used to study it.

The normal momentum exchange with the surface, which jumps from zero to one-half the free-stream momentum per molecule upon the initial collision, reaches a maximum at the end of this zone; it varies little in the transition region, because the further conversion of stream-wise momentum into cross-stream-directed momentum is roughly a geometric progression in terms of the number of collisions. Gross calculations for the density of tertiary collisions were carried out, and these indicated that indeed the total mass and the corresponding momentum flux to the plate extend smoothly (asymptotically) past the maximum of the en flux into the transition region.

It is clear that the normal momentum flux to the surface must

reach a plateau. The foregoing arguments indicate that this is of the order of the flux existing at the edge of the initial collision zone.* We shall assume this in the following discussion of the induced pressure.

* Note that it was assumed that all the $(en)_2$ molecules reach the wall. It was shown that tertiary collisions are thereby approximately accounted for in what concerns the downward momentum flux intercepted by the surface.

III. THE INDUCED PRESSURE

A number of physically significant flow properties (wall shear, velocity profiles, second approximation to the local density, etc.) can be derived from the previous calculations. In this Memorandum we shall discuss primarily the problem of the pressure at the surface. This is the only quantity that has been measured under conditions which fit approximately the assumptions of this analysis and, therefore, the one for which some verification of the results can be provided. The most recent and the most complete series of tests is that reported by Nagamatsu and Sheer.⁽¹⁾ The measurements are reproduced in Fig. 7. The major portion of the measurements are well into the continuum regime; however, the curves do show a well-defined plateau near the leading edge. According to what was stated previously, this maximum occurs in the transition regime, and its magnitude equals approximately the pressure at the edge of the initial-collision domain.

To calculate the wall pressure we must consider the free-stream molecules (Eq. (14)) contributing $\rho_n m \bar{v}_T \bar{v}_T$ to the normal momentum per unit surface plus the en molecules (Eqs. (16) and (23)), carrying approximately $1/2 n_{en} m V_e (V_1 - V_e/V_n)$ momentum per unit surface, and finally the reaction due to the emission from the wall, $n_e m V_e$. The expression for the induced pressure becomes

$$2 \frac{P}{P_\infty} = e^{-\frac{\alpha}{M^T}} \left[1 + 1/2 \left(1 - \frac{V_e}{V_n} \right) \frac{M'^2}{\alpha} \left(e^{-\frac{\alpha}{M^T}} \begin{pmatrix} -\alpha \\ e-1 \\ -1 \end{pmatrix} \right) \right] + M' \frac{V_e}{V_n} \quad (26)$$

We shall begin by studying the induced-pressure maximum in order

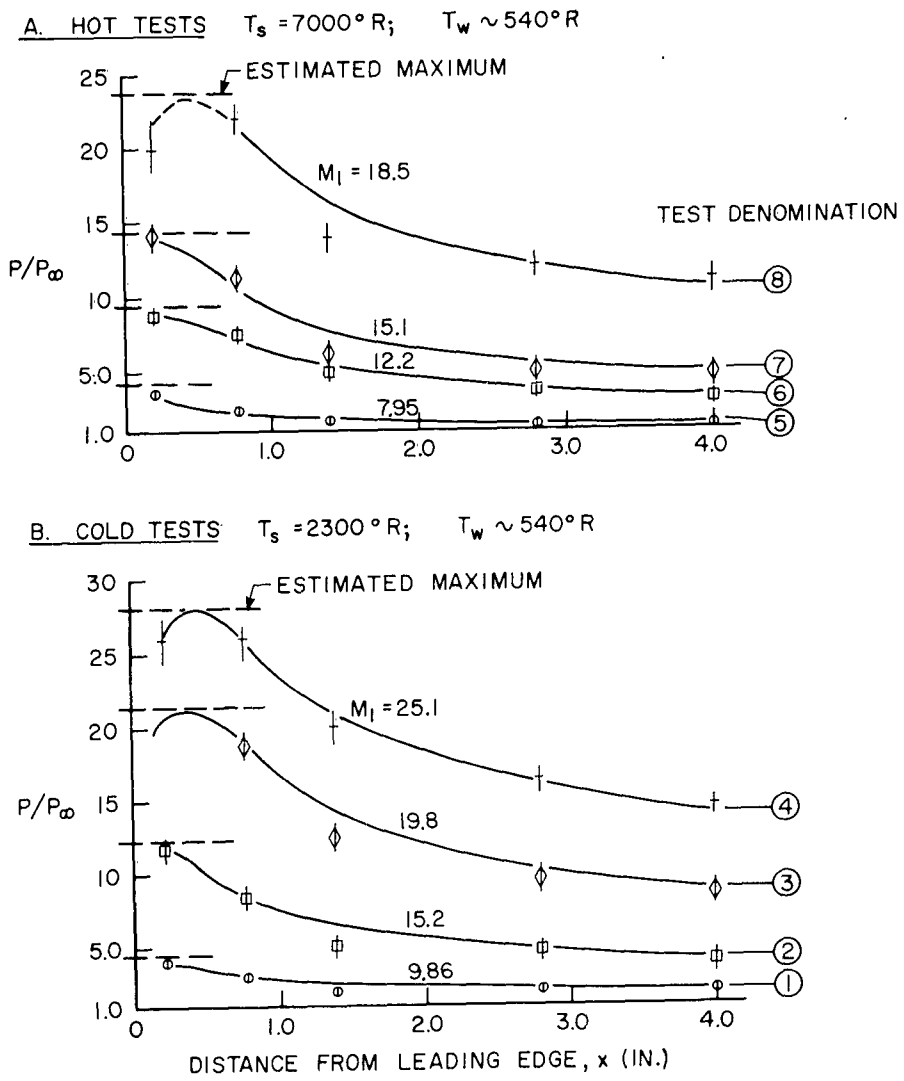


FIG. 7 — MEASUREMENTS OF INDUCED PRESSURE⁽¹⁾

to adjust the numerical constants (which were approximated throughout the analysis) and to verify the truth of the model we formulated.

We remark that the pressure maximum is expected to occur at a value of α larger than, but on the order of, unity. However, α/M' is expected to remain small because the Mach number must be large. Accordingly, expanding the exponential in α/M' and carrying the analysis out to first order in that parameter, we find that the maximum of Eq. (26) occurs at α_{\max} given by the solution of

$$\frac{2}{M'^2 \left(1 - \frac{v_e}{V_n}\right)} = e^{-\alpha_{\max}} \left(1 + \frac{\alpha_{\max} - 1}{M'}\right) \quad (27)$$

Therefore

$$\begin{aligned} \alpha_{\max} &= \ln \left[M'^2 \frac{1}{2} \left(1 - \frac{v_e}{V_n}\right) \right] + \ln \left(1 + \frac{\alpha_{\max} - 1}{M'}\right) \\ &\approx \ln \left[M'^2 \frac{1}{2} \left(1 - \frac{v_e}{V_n}\right) \right] - \frac{1}{M'} \\ &\approx \ln \left[M'^2 \frac{1}{2} \left(1 - \frac{v_e}{V_n}\right) \right] \end{aligned} \quad (28)$$

where the successive forms of Eq. (28) represent successive numerical approximations which are allowable for α/M' small and M' large.

By the same degree of approximation, Eq. (26) can be expanded to read

$$\begin{aligned} 2 \left[\frac{P}{P_\infty} - 1 \right] &= \frac{1}{2} M' \left(1 + \frac{v_e}{V_n}\right) - \frac{1}{2} M' \left(1 - \frac{v_e}{V_n}\right) e^{-\alpha} \\ &\quad - \frac{\alpha}{M'} \left(1 + \frac{1}{4} M' \left(1 - \frac{v_e}{V_n}\right)\right) - e^{-2\alpha} \end{aligned} \quad (29)$$

Combining Eqs. (28) and (29), the expression for the maximum induced pressure becomes*

$$\begin{aligned} \left(\frac{\Delta P}{P_\infty}\right)_{\max} &= \left(\frac{P - P_\infty}{P_\infty}\right)_{\max} \\ &= \frac{1}{2} \left\{ \frac{1}{2} M' M' \left(1 + \frac{V_e}{V_n}\right) - \frac{\alpha_{\max}}{M'} \left[1 + \frac{1}{4} M' \left(1 - \frac{V_e}{V_n}\right)\right] \right. \\ &\quad \left. - \frac{M' + \alpha_{\max}}{M' + \alpha_{\max}} - 1 \right\} \\ &\approx \frac{1}{2} \left\{ \frac{1}{2} M' \left(1 + \frac{V_e}{V_n}\right) - \frac{1}{4} \left(1 - \frac{V_e}{V_n}\right) \ln \left[M'^2 \frac{1}{2} \left(1 - \frac{V_e}{V_n}\right) \right] - 1 \right\} \end{aligned}$$

By comparing this approximate form to the full Eq. (26), we find an error of less than 5 per cent at most in the range of the experimental data ($M_0 > 8$).

DISCUSSION AND COMPARISON WITH DATA

Before proceeding in a comparison of the results of this theory to the available experimental points, it is necessary to introduce some proportionality constants, omitted in the analysis, by the assumption of a two-dimensional, nearly Newtonian molecular model. The nonlinear form of Eq. (30) in both independent variables M' and V_e/V_n makes this difficult to do by purely graphical means. However, a physical analysis of the model provides the following guide:

*The free-stream pressure, P_∞ , is defined herein in terms of the momentum exchange with an element of surface parallel to the flow in equilibrium with it; that is

$$P_\infty = (\rho \bar{v}_T) + n_e \bar{v}_T = 2\rho \bar{v}_T \bar{v}_T.$$

In the course of the analysis three separate molecular families were defined, and their interactions were described in terms of the characteristic velocities of the families. Each of these characteristic velocities is an unspecified average over the velocity-distribution function of the family, and, moreover, in each case the motion is assumed to be two-dimensional (neglecting the component parallel to the leading edge).

We are, therefore, led to introduce the following proportionality constants:

a. The free-stream family is described by the parameter M' , which is a sort of molecular speed ratio based on the mean directed thermal velocity of the gas. We set it proportional to the true Mach number as follows

$$M' = \frac{V_n}{\bar{v}_T} = CM_o$$

b. The surface-emitted family is characterized by the mean velocity V_e . Eliminating the free-stream velocity, we write

$$\frac{V_e}{V_n} = \frac{V_e}{\bar{v}_T} \frac{\bar{v}_T}{V_n} = \frac{1}{CM_o} \left(\frac{V_e}{\bar{v}_T} \right)$$

Both V_e and \bar{v}_T are averages over distributions of the same character, and their ratio needs no additional constants. However, V_e is not generally known. Instead, the surface temperature is known and thus

$$\frac{V_e}{\bar{v}_T} = F \sqrt{\frac{T_w}{T_\infty}}$$

where F is essentially the inverse thermal-accommodation coefficient.

It should be recalled that the entire analysis (with Model V) has made the assumption $\theta = 0$, which corresponds to an assumption of a normal momentum-accommodation coefficient of unity (diffuse reflection).

It should also be borne in mind that the "cold wall" assumption implied here requires that $V_e/\bar{v}_T \sim 1$; and therefore not only $T_w/T_\infty \sim 1$, but also F must be on the order of unity.

Combining these definitions, the velocity ratio, V_e/V_n , can also be expressed in terms of the wall-to-stagnation temperature ratio

$$\frac{V_e}{V_n} = \frac{F}{C} \sqrt{\frac{1}{M_o^2} + \frac{\gamma - 1}{2}} \sqrt{\frac{T_w}{T_s}}$$

$$\lim_{M \rightarrow \infty} \frac{V_e}{V_n} = \frac{F \sqrt{(\gamma - 1)/2}}{C} \sqrt{\frac{T_w}{T_s}}$$

This formulation is convenient for comparison with data such as those in Ref. 1, which consist of series of tests at constant T_w/T_s . However, the use of the ratio T_w/T_∞ as a basic variable probably would be preferable in future analytic as well as experimental work.

c. The scattered family is described by the velocity V_{en} , again a two-dimensional characteristic. Accordingly, we set

$$\frac{V_{en}}{V_n} = D \left(1 - \frac{V_e}{V_n} \right) = D \left(1 - \frac{F}{C} \sqrt{\frac{\gamma - 1}{2}} \sqrt{\frac{T_w}{T_s}} \right)$$

where D absorbs the factor 1/2 used thus far. There is, of course, a cross-coupling between the scattered family and the wall-emission temperature.

We have, consequently, four basic constants:

C, D= numerical proportionality factors relating
to the molecular model

θ , F= surface-interaction parameters, essentially
the normal momentum (σ) and inverse thermal-accommodation coefficients (α)

The first two stem from the simplifications of this analysis and could be calculated at the cost of numerical effort. The last two (in this or in another form) are the ever-present kinetic surface-interaction parameters which would require the assumption of a surface-interaction model such as Schamberg's,⁽¹⁰⁾ and this remains the principal unknown in free-molecule and near-free-molecule theory.

In the following we shall make initially the common assumption that there is perfect surface accommodation, i.e.,

$$\bar{\theta} = 0 \quad F = 1$$

and use the two available empirical equations describing the induced pressure (two series of tests each at constant T_w/T_s) to evaluate C and D. The procedure and the evidence that F is not unity in these tests, as well as remarks concerning the effect of this on the present comparison between the theory and the experiment, are

given in the Appendix.

Introducing these constants into Eq. (30) and rearranging, we obtain

$$\left(\frac{\Delta P/P_\infty}{M_o}\right)_{\max} = \frac{CD}{2} \left(1 - \frac{F}{C} \sqrt{\frac{\gamma-1}{2}} \frac{T_w}{T_s}\right) \left\{ 1 - \frac{1}{2CM_o} \left[2 \ln M_o + \ln \left[CDC \left(1 - \frac{F}{C} \sqrt{\frac{\gamma-1}{2}} \frac{T_w}{T_s}\right) \right] \right] \right\} \quad (31)$$

$$+ \frac{1}{2} \left(F \sqrt{\frac{\gamma-1}{2}} \frac{T_w}{T_s} - \frac{1}{M_o} \right)$$

$$\alpha_{\max} = 2 \ln M_o + \ln \left[CDC \left(1 - \frac{F}{C} \sqrt{\frac{\gamma-1}{2}} \frac{T_w}{T_s}\right) \right] \quad (32)$$

Using the procedure described in the Appendix and the data of Ref. 1* we find the most reasonable estimate of the constants to be

$$C = 0.33$$

$$D = 25$$

Equation (31) is shown graphically in Fig. 8 in a comparison with the experimental measurements. The correlation is remarkably

* There is also available data showing the plateau of hypersonic induced pressure obtained by J. Aroesty: Pressure Distribution on Flat Plates at Mach 4 and Low Density Flow, Univ. of California Inst. Eng. Res. Rep. HE 150-157, July 1958. This is not used for comparison with this theory because the tests were conducted on an insulated model with nearly stagnation wall temperature, and the condition $V_e/V_n \ll 1$ implied in the analysis was definitely not met. Qualitatively, however, there are no contradictions between Aroesty's measurements and the present results.

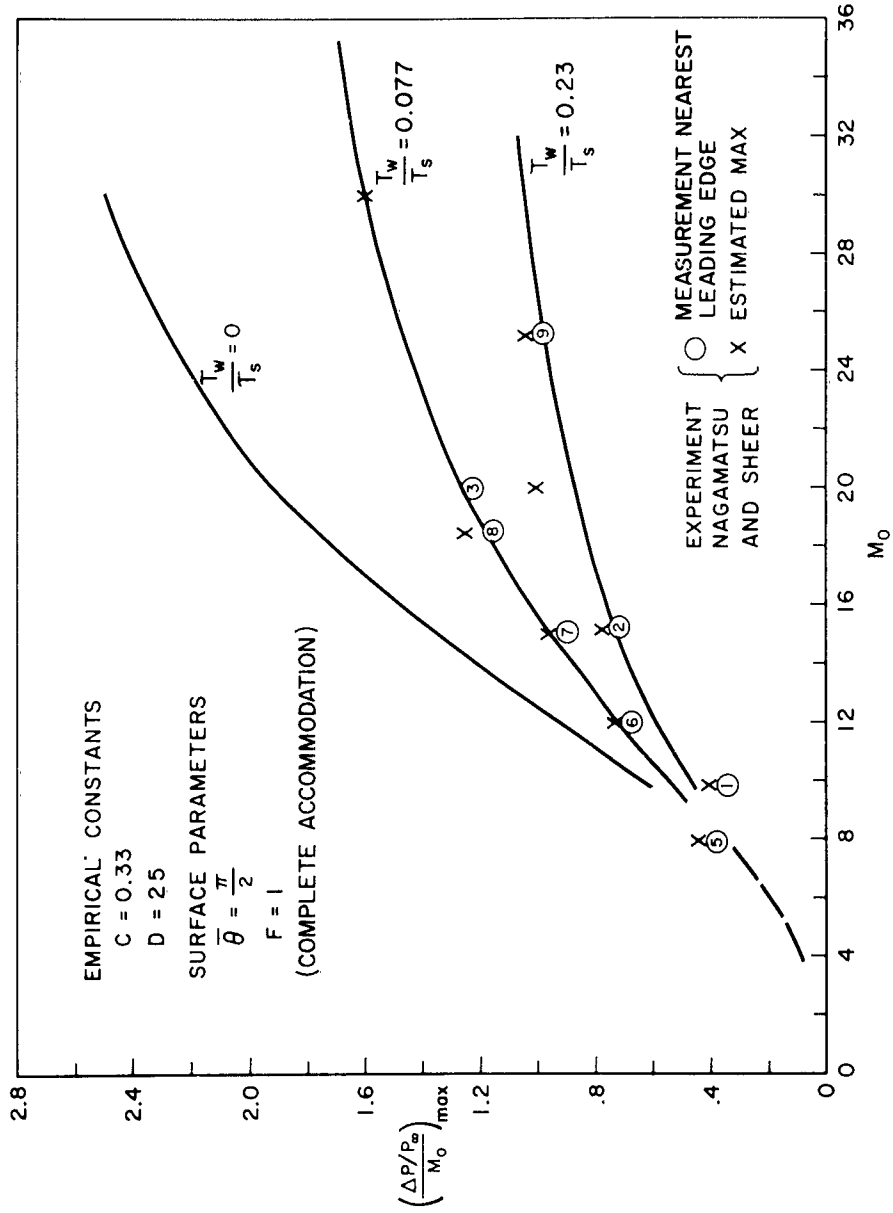


FIG. 8 — COMPARISON OF EXPERIMENTAL AND THEORETICAL RESULTS

good, since it covers a large range of both independent parameters of the problem, which enter the equation in a nonobvious way. However, the quantitative results should not be overemphasized for several reasons: The molecular model is approximate; the experimental measurements are not certain (it is pointed out in the Appendix how an even better fit can be obtained if one assumes, for example, a partial accommodation to surface conditions); and finally, some of the test conditions do not comply very closely with the conditions for validity of the analysis--a high Mach number and a very low wall temperature.

Perhaps the most significant result is the prediction of a decrease in the maximum induced pressure with an increase of wall-to-stagnation temperature ratio. This trend seems definitely to be verified by the experiment. On the other hand, it contradicts the prediction of the merged-layer analysis based on slip-free continuum concepts.⁽¹¹⁾ In order to bring this fact into focus, the data, the present kinetic theory, and Oguchi's⁽¹¹⁾ wedge-like-flow solution are compared in Fig. 9. It appears that they coincide for the particular case of $T_w/T_s = 0.08$, the only experimental test discussed by Oguchi, but when applied to the low-stagnation-temperature case his results diverge significantly from both the data and the present results.

It is also interesting to observe that the present theory predicts in the high-Mach-number case a linear variation of the induced-pressure ratio with Mach number

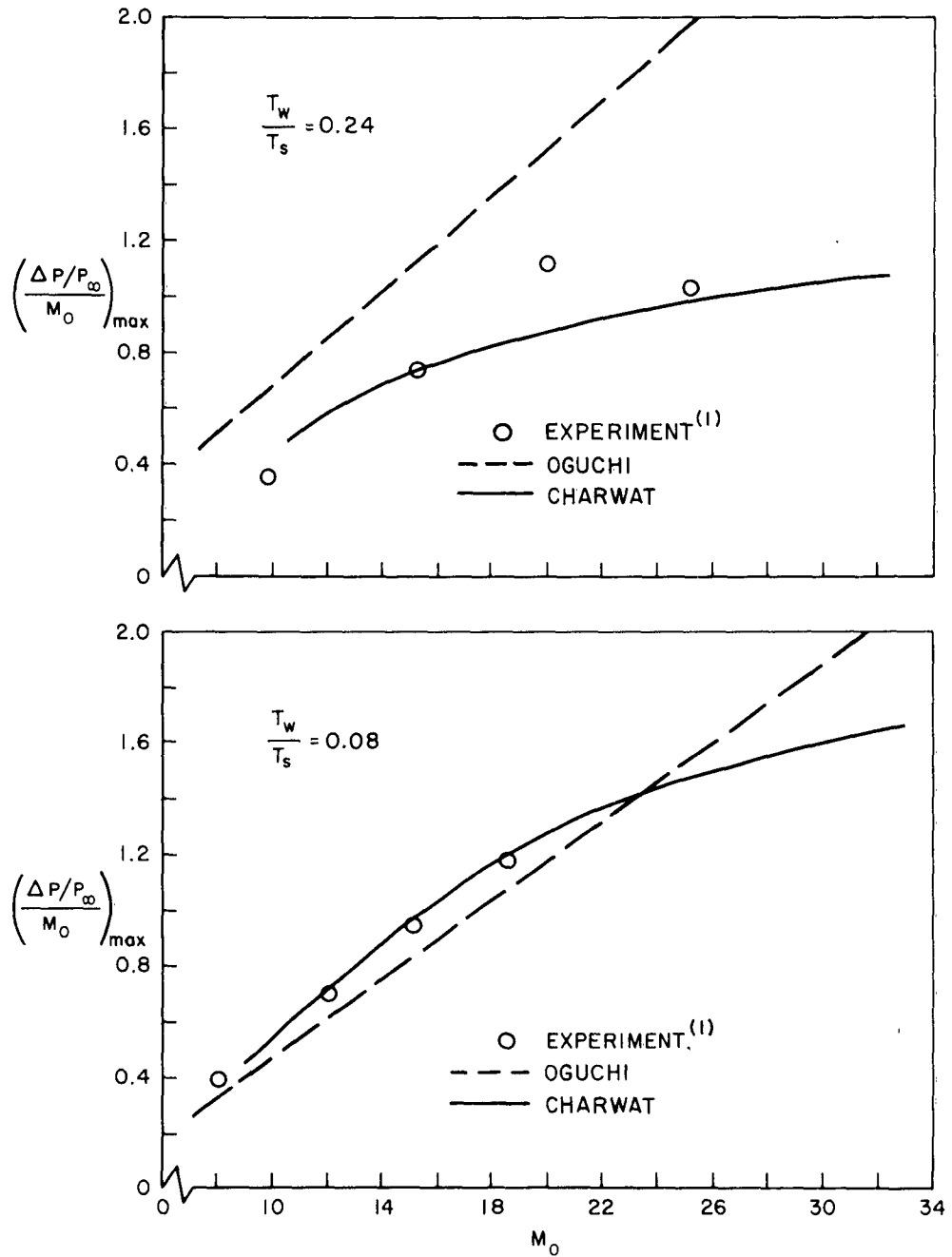


FIG. 9 — COMPARISON OF DATA AND LEADING-EDGE-INTERACTION THEORIES FOR VARYING T_w/T_s

$$\lim_{M_o \rightarrow \infty} \frac{\Delta P}{P_\infty} = \left[\frac{1}{2} \sqrt{\frac{\gamma - 1}{2}} \frac{T_w}{T_s} (1 - D) + \frac{CD}{2} \right] M_o$$

while Oguchi's result gives a parabolic increase of this ratio

$$\lim_{M \rightarrow \infty} \frac{\Delta P}{P_\infty} = \frac{\gamma - 1}{2} G \left(\frac{T_w}{T_s} \right) M_\infty^2$$

where G, a function of T_w/T_s , lies between $1/4$ and $\pi/4$. The former seems more reasonable than the latter on the ground of physical arguments.

The initial pressure rise (first-order in α) is easily derived from Eq. (26). In terms of the three independent parameters of the problem, the Mach and Reynolds numbers and the wall-to-free-stream temperature ratio, and where A and B are numerical constants, it is

$$\begin{aligned} \left(2 \frac{P}{P_\infty} \right)_{\alpha > 0} &= \frac{1}{2} M' \left(1 - \frac{V_e}{V_n} \right) \alpha + M' \frac{V_e}{V_n} + 1 \\ &\simeq (A) \operatorname{Re} M_o \left(\sqrt{\frac{T_\infty}{T_w}} - \frac{1}{M_o} \right) + (B) \sqrt{\frac{T_w}{T_\infty}} + 1 \end{aligned} \quad (34)$$

At a fixed Mach number and increasing rarefaction ($\operatorname{Re} \rightarrow 0$), the induced pressure rise is dominated by the retroforce due to the wall emission (the second term); this is in accord with free-molecule theory. With increasing density, that is, towards continuum flow ($\operatorname{Re} \rightarrow \infty$), the slope of the initial pressure rise tends to infinity. However, the maximum induced pressure at $\alpha = \alpha_{\max}$ remains finite regardless of density, as it depends only on the Mach number and the wall-to-free-stream temperature ratio.

In concluding this discussion, we note that in the domain of kinetic flows all the incident fluxes are convected to the surface by the molecules themselves. Therefore, when expressed as a ratio to the free-stream (free-molecule) flux, all the incident transfer properties will have the form

$$\frac{X_i}{X_{FM_i}} = e^{-\frac{\alpha}{M'}} + \frac{X_{en}}{X_{FM_i}} \frac{n_{en}}{n_e}$$

where X stands for the property under consideration. We have

$$\frac{X_{en}}{X_{FM_i}} = \begin{cases} \frac{1}{2} M' \left(1 - \frac{v_e}{v_n} \right) & \text{Normal momentum* (pressure)} \\ \frac{1}{2} \left(1 - \frac{v_e}{v_n} \right) & \text{Tangential momentum (shear)} \\ \frac{1}{2} \left(1 - \frac{v_e}{v_n} \right)^2 & \text{Kinetic energy (heat transfer)} \end{cases}$$

Similarly, the reflected (surface-emitted) flux can be expressed as $\frac{X_w}{X_{FM_i}}$ where, for the model considered,

$$\frac{X_w}{X_{FM_i}} = \begin{cases} + M' \frac{v_e}{v_n} & \text{Normal momentum} \\ 0 & \text{Tangential momentum} \\ - \frac{v_e}{v_n}^2 & \text{Kinetic energy} \end{cases}$$

*Note that $P_{FM_i} = \frac{1}{2} P_\infty = \rho \bar{v}_T \bar{v}_T$.

The difference $\frac{X_i - X_w}{X_{FM_i}}$ is shown in Fig. 10 for specific values of the independent parameters. Note that the relative magnitude as well as the location of the maximum of these curves depends on the choice of the proportionality constants, C and D, and the surface-accommodation constant, F. The heat transfer, in particular, is sensitive to the value of this constant. In order to demonstrate this effect, two sets of curves are shown.

In principle, measurements of the heat-transfer plateau such as are being currently obtained* could provide the third empirical equation from which C, D, and also F could be determined simultaneously. This is discussed in more detail in the Appendix in connection with the preliminary heat-transfer data that are available.

SECOND APPROXIMATION TO n_{en}

In the foregoing discussion, the density of the surface emission was assumed to be constant along the plate. A second iteration on n_e can be carried out easily for the initial zone to give an estimate of the effect of this assumption. To the second order, the local surface emission equals the local flux of the free stream, n_n , and the first-scattered molecules, n_{en} , collected by the surface; that is

* Personal communications from Dr. H. T. Nagamatsu, General Electric Research Laboratories, Schenectady, N. Y.

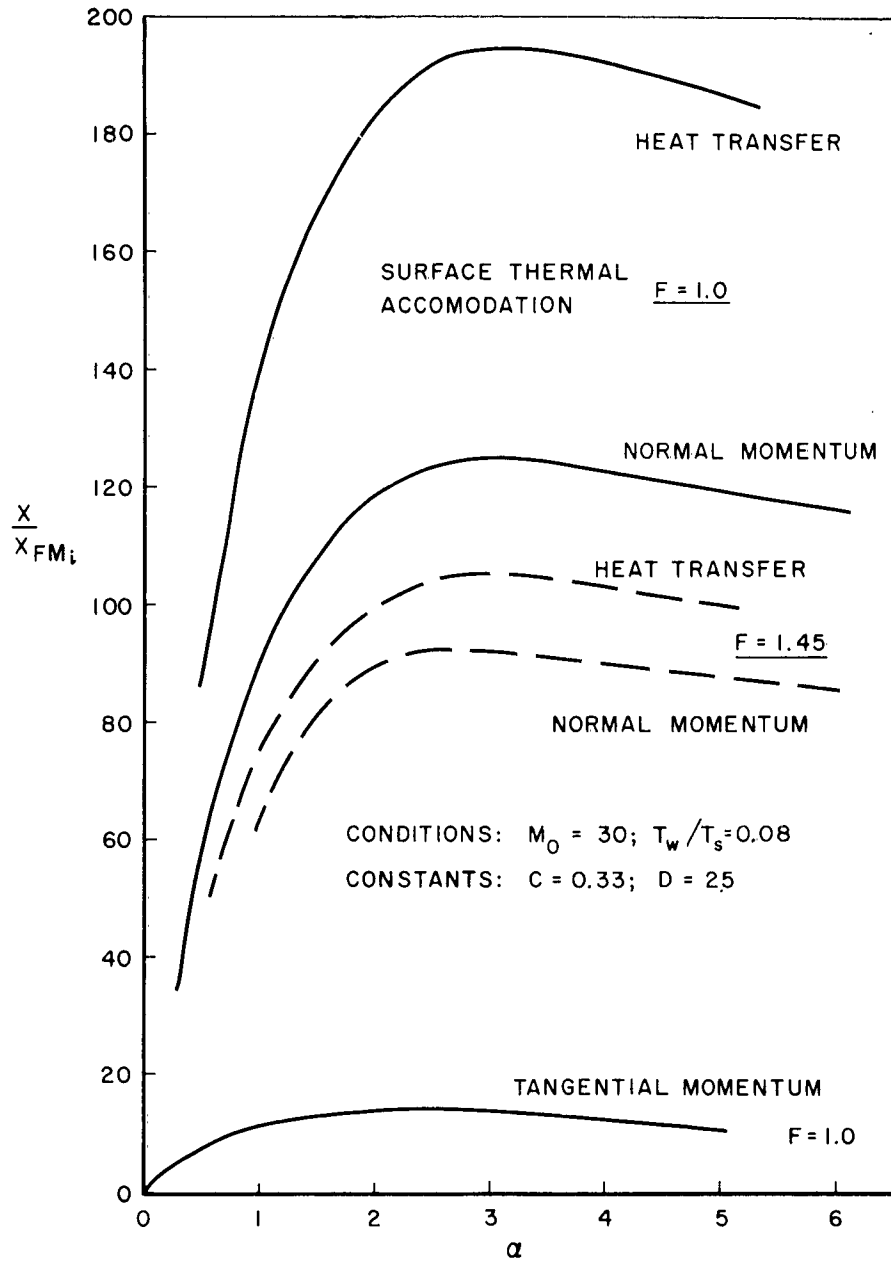


FIG.10 — GENERALIZED TRANSFER PROPERTIES IN THE LEADING-EDGE REGION. EFFECT OF SURFACE THERMAL ACCOMODATION

$$n_e^{(2)} = n_n^{(1)} + n_{en}^{(1)}$$

The result is, for the initial zone for which both $\alpha/M \ll 1$ and $e^{-\alpha} \simeq (1 - \alpha)$

$$\begin{aligned} n_{en}^{(2)} &= n_{en}^{(1)} + \int_0^{\xi_m} \alpha \frac{dn_e^{(1)}}{d\xi} d\xi \\ &= n_{en}^{(1)} + \rho V_n \left(1 - e^{-\frac{\alpha}{M'}} \right) \\ &\sim n_{en}^{(1)} + \frac{\alpha}{M'} \rho V_n \end{aligned}$$

The second term represents the increase of the flux due to the coupling between the surface emission and the density of the first scatterings.

Continuing as outlined for the first-order analysis, the pressure on the surface downstream of the leading edge ($x < L_e$) is

$$\begin{aligned} 2 \frac{\Delta P^{(2)}}{P_\infty} &= 2 \frac{\Delta P^{(1)}}{P_\infty} + 1/2 M' \alpha \left(1 + \frac{v_e}{v_o} \right) \\ &= M' \left(\alpha + \frac{v_e}{v_o} \right) \\ &= A^{(2)} M' Re \sqrt{\frac{T_\infty}{T_w}} + B^{(2)} \sqrt{\frac{T_w}{T_\infty}} \end{aligned} \tag{34}$$

The second approximation gives essentially the same form for the initial pressure rise, which is dominated by the product $M'Re$, but the slope of the second-order approximation (the constant $A^{(2)}$) is higher by a factor of about 2.

SURFACE SHEAR NEAR THE LEADING EDGE

By following the procedure already established, we can obtain the first approximation to the local shear coefficient by adding the contributions due to the incident flux ($m_0 v_T v_n$) to those due to the scattered flux ($m_{en} v_{en} u_{en}$). The emitted molecules do not carry any tangential momentum in the case of the simple normal beam-emission model (Model V) considered here.

We find without difficulty

$$C_f = \frac{\tau}{1/2 \rho_n V_n^2} \tag{35}$$

$$= e^{-\frac{\alpha}{M'}} \left\{ \frac{2}{M'} + \frac{1}{\alpha} \left[e^{-\frac{\alpha}{M'}} (e^{-\alpha} - 1) - 1 \right] \left(1 - \frac{v_c}{v_n} \right) \right\}$$

This expression reduces to the free-molecule skin friction

$$C_{f_{FM}} = \frac{2}{M} \tag{36}$$

when L_{e0} tends to infinity for any finite value of x . This is indeed the correct form for the molecular models considered.

As before, simplified expression for the hypersonic case in the initial-collision domain, and for the extreme leading-edge

region can be derived by expanding the exponentials

For $\frac{\alpha}{M} \rightarrow 0$

$$\frac{C_f}{C_{f_{FM}}} = 1 + 1/2 \left(1 - \frac{V_e}{V_n} \right) (1 - e^{-\alpha}) \quad (37)$$

For $\alpha \rightarrow 0$

$$\frac{C_f}{C_{f_{FM}}} = 1 + 1/2 \left(1 - \frac{V_e}{V_n} \right) \alpha \quad (38)$$

In terms of the Mach and Reynolds numbers the last expression is (A and B are again numerical constants)

$$\frac{C_f}{C_{f_{FM}}} = 1 + (A) \operatorname{Re} \sqrt{\frac{T_\infty}{T_w}} - (B) \frac{\operatorname{Re}}{M^2} \quad (39)$$

We find thus that the skin friction behaves like the pressure. There is an initial increase of local friction downstream of the leading edge, a maximum, and finally a decrease in the transitional zone. This is due to the flux of first-scattered molecules to the surface, which overrides the decrease of the flux of the incident molecules and the decrease of momentum per molecule of the scattered molecules compared to the incident ones.

It is notable that this result is characteristic of the high-Mach-number case. Although this analysis is not strictly valid for low

Mach numbers because of the basic assumptions discussed previously, the trend is nonetheless evident. If one sets $M = 0$ in Eq. (35)

$$\lim_{M \rightarrow 0} \frac{C_f}{C_{f_{FM}}} = 1 - \frac{\alpha}{M} \sim 1 - \frac{Re}{M} \sqrt{\frac{T_\infty}{T_w}} \quad (40)$$

At low M the friction coefficient decreases immediately downstream of the leading edge. This is the same result as that of Liu.^{(12)*} Liu neglects the change in the space-density distribution of molecules brought about by the interactions and therefore does not obtain the term which increases C_f at all. In this sense his physical model is only valid for the near-stationary case; moreover, in the numerical approximation he sets $M < 1$ in his calculation.

HEAT TRANSFER, SLIP, AND TEMPERATURE JUMP

This model is valid only for the highly cooled plate ($V_e \ll V_o$; $T_w < < M^2 T_\infty$), and therefore a recovery temperature cannot be calculated. The variation of the local heat-transfer coefficient in the initial-collision zone for a fixed wall temperature (fixed V_e) is of course qualitatively similar to the variation of the induced pressure. Thus, we expect a rapid rise to a maximum followed by a decay to the value of continuum theory. Incidentally, a constant V_e would require a particular heat-absorption schedule (or a particular variation of thermal accommodation to the plate).

A slip velocity and a temperature jump at the wall can be calculated simply from the foregoing. The physical slip velocity for the simple first-order model investigated here is

* Liu's function G is approximately proportional to M so that his correction term $(Re/M^2) G$ exhibits the same general dependence on the flow parameters.

$$U_s = \frac{1}{n_e + n_{en}} \left(n_e V_n + n_{en} \frac{1}{2} V_n \right)$$
$$= V_n \frac{1 + \frac{1}{2} \frac{n_{en}}{n_e}}{1 + \frac{n_{en}}{n_e}}$$

which can be gotten directly from Fig. 6 or Eq. (23). It is seen that in the domain of validity of this analysis the slip velocity decays from free stream to about 75 per cent of free-stream velocity at hypersonic speeds. The decrease of U_s is monotonic from the leading edge. Now, in terms of slip-flow theory, the wall shear is proportional to the slip velocity, which is taken to be proportional to the mass velocity gradient at the wall. The present analysis indicates an inconsistency in the slip-flow assumption if it is to be extended into near-free-molecule flow, because very near the leading edge in hypersonic flow the shear is shown to increase while U_s decreases.

IV. EMPIRICAL EXTENSION OF THE RESULTS

The present analysis is valid in the initial-collision domain only, but hopefully it can also be used as a framework for further semiempirical correlations. There is one critical point on the hypersonic interaction curves: namely, the continuum limit of the constant-pressure plateau (marked on the curves of Fig. 11 by a vertical arrow) which, if it were predictable, would allow the induced pressure to be drawn for all values of the flow parameters.

A schematic induced-pressure curve is drawn as an insert in Fig. 12. One distinguishes the leading-edge-pressure rise to a hypersonic interaction parameter, χ_s , corresponding to the edge of the initial-collision region. Following this region, there is the constant-pressure plateau between values χ_s and χ_c of the interaction parameter. This region was previously identified with a transition in which the kinetic motion in the disturbed layer readjusts itself to the equilibrium condition characteristic of a continuum boundary layer. From this point on, the further growth and the displacement effect of the boundary layer are governed by shear transfer and mass continuity as postulated in the continuum analysis of interaction theories.

The edge of the initial collision zone, Eq. (28), is determined physically by the convective distance to undergo a fixed number of collisions. The parameter which describes this is the slip parameter⁽¹⁾

$$\left(\frac{M_o}{\sqrt{Re}} \right)_s = \frac{\chi_s}{M_o^2} = 0.69 \left[\frac{M_o}{\sqrt{\frac{T_w}{T_s} \alpha_{max}}} \right]^{1/2} \quad (41)$$

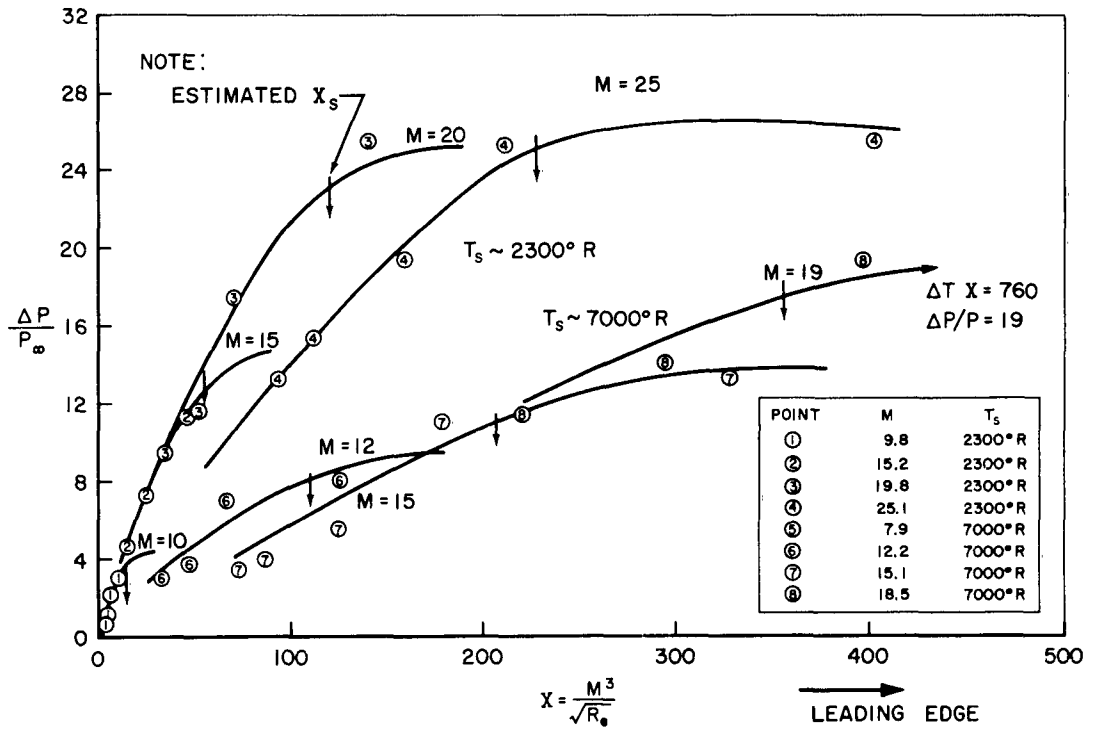


Fig. II — Induced-pressure measurements versus continuum-interaction parameter⁽¹⁾

NOTE:
TYPICAL INDUCED
PRESSURE VARIATION

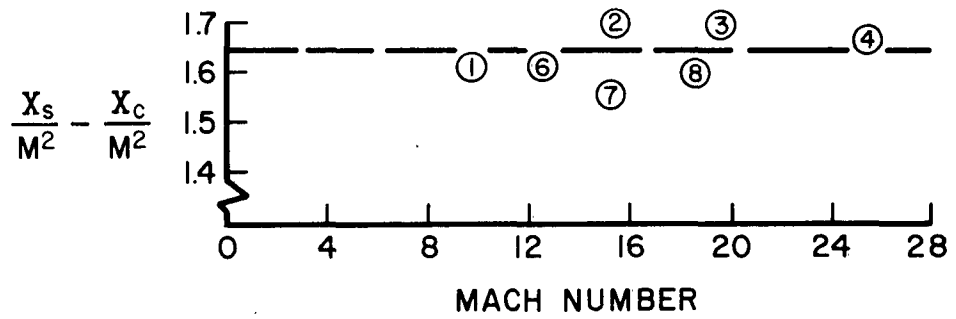
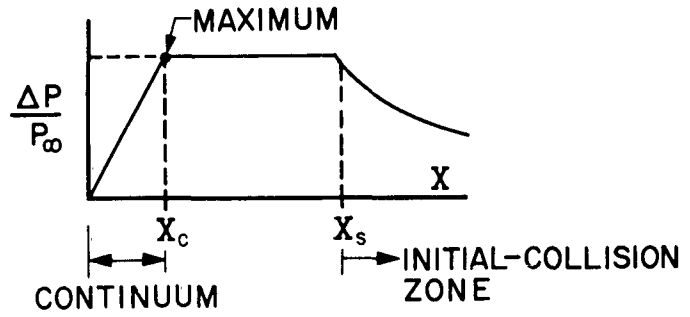


Fig.12 — The extent of the pressure plateau

where the second equality is obtained from Eq. (28). The Mach number dependence of χ_s/M^2 reflects the streamwise distortion (stretching) of the zone of first collisions.

We postulate that the extent of the transition zone is also determined by a fixed number of collisions, which are required to establish a new equilibrium. Since the molecular motion in the transition region is predominately along 45-deg lines and both the normal and streamwise components of the molecular paths are of the same order, we do not expect a streamwise distortion of this zone. The convective distance required for the fixed number of collisions is then a constant, and we seek a correlation in terms of

$$\frac{\chi_s}{M_o^2} - \frac{\chi_c}{M_o^2} = \text{Constant} \quad (42)$$

Figure 12 shows the results. (The use of the Mach number as the ordinate is purely a means of displaying the data.) Indeed, within the accuracy with which the continuum edge of the transitional plateau can be defined, Eq. (42) is well substantiated with a proportionality constant of about 1.6. Note that the data include a considerable range of Mach numbers and an independent variation of stagnation temperatures.

One is also tempted to use the results of this analysis to plot velocity or density profiles through the disturbed layer. This can, of course, be done numerically. However, we believe that more precise results than those which can be derived by an inspection of Fig. 5 would not be significant; inasmuch as good arguments can be given for the validity of the wall-flux calculation, the details of the

field are probably grossly oversimplified by this model. The one result worth noting is the wedge-like growth of the disturbed zone; a sort of oblique characteristic line defined by a maximum in the gradient of the density of disturbed molecules can be seen to be along the line $x = y$ (hyperthermal flow), regardless of density. This line should not be identified, however, with the continuum gas-dynamic oblique shock without further study. Using this first approximation as an indication, we note also that the maximum gradient of the total density (emitted, scattered, and incident families) grows in an exponential fashion from the leading edge and does not lie on the line $x = y$. This is the line which would show up, for example, on a Schlieren photograph.

Appendix

EVALUATION OF CONSTANTS

The tests of Ref. 1 consist of 2 sets of 4 runs each at varying Mach numbers, each set at constant wall-to-stagnation temperature. From Eq. (33) we find that there is to be expected an asymptotic limit of the ratio $\frac{\Delta P/P}{M_o}$ as M_o goes to infinity*

$$\lim_{M_o \rightarrow \infty} \frac{\Delta P/P}{M_o} = \frac{CD}{2} \left[1 - \frac{F}{C} \sqrt{\frac{\gamma-1}{2} \frac{T_w}{T_s}} \right] + \frac{F}{2} \sqrt{\frac{\gamma-1}{2} \frac{T_w}{T_s}} \equiv L \quad (A-1)$$

It is convenient to use L in the iterative process, although there are no data available to determine it directly from the experiment (which would be convenient).

We have

$$CD = \frac{2L - F \sqrt{\frac{\gamma-1}{2} \frac{T_w}{T_s}}}{1 - \frac{F}{C} \sqrt{\frac{\gamma-1}{2} \frac{T_w}{T_s}}} \quad (A-2)$$

Having two independent tests allows C · D to be eliminated. It follows that letting

$$T = \sqrt{\frac{\gamma-1}{2} \frac{T_w}{T_s}}$$

$$C = \frac{2F (T_1 L_1 - T_2 L_2)}{F (T_1 - T_2) + 2(L_2 - L_1)} \quad (A-3)$$

As we stated in the text, we begin by assuming

$$F = 1; \gamma = 1.4$$

*L is used here as a shorthand notation, as per Eq. (A-1).

(This third constant could not be unambiguously found from only two test series.) There is some question as to whether $\gamma = 1.4$ for both tests, but any departure could be absorbed in the unknown constant F. The procedure used is this:

- a. Assume C and L_2 (for the hot tests); solve for CD from Eq. (A-2); solve Eq. (A-1) at two Mach numbers and compare with experiment.
- b. Solve for L_1 from Eq. (A-3) (for the cold tests); solve Eq. (A-1) at two Mach numbers and compare.

Several tries lead to the curves shown in Fig. 6, with the values

$$F = 1$$

$$\gamma = 1.4$$

$$C = 0.33$$

$$D = 25$$

Effect of Changing F

Note that this method of simultaneous solution (Eqs. (A-1), (A-2), and (A-3)) makes the variables C, D, and F interdependent. To demonstrate this, Fig. A-1 shows the effect of varying F at constant C. One has

$$C = 0.33 \quad - \quad F = 1 \quad , \quad D = 25$$

$$C = 0.33 \quad - \quad F = 1.2 \quad D = 27$$

This new value of F corresponds to thermal accommodation less than unity (approximately $1/F = 80$ per cent). It is seen that this improves the simultaneous correlation of theory and experiment.

The small change in F (decrease of the accommodation coefficient) did not destroy the fit for the hot tests. However, were F to be

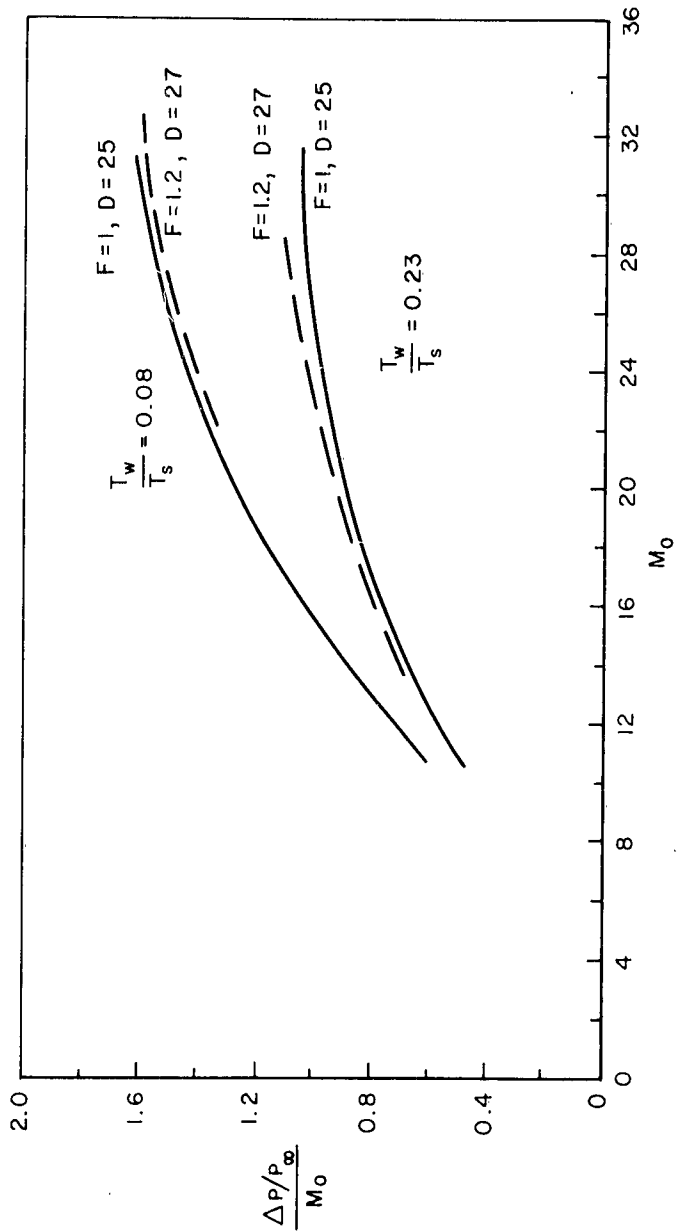


FIG. A-1 — THE EFFECT OF VARYING F AT CONSTANT C = 0.33

increased further, C would need to be decreased. Numerically, the fit would be improved for both tests, but the term

$$\frac{F}{C} \sqrt{\frac{\gamma-1}{2} \frac{T_w}{T_s}}$$

would keep increasing to values close to unity. This invalidates the fundamental assumption $V_e/V_n \ll 1$ and, therefore, the whole analytical result.

Discussion of Heat-Transfer Results

We turn now to the heat-transfer measurements available to date.* There are two tests which show clearly the existence of a heat-transfer plateau at about the same distance from the leading edge as the pressure plateau. Their magnitudes are

$$C_H M^3 \cong 140 \text{ at } M = 19.2 \quad T_w/T_s = 0.083$$

$$C_H M^3 \cong 320 \text{ at } M = 25.1 \quad T_w/T_s = 0.212$$

where C_H is the Stanton number based on the net heat transfer to the wall.

As outlined in the text (see Fig. 8), we form the ratio C_H/C_{HFMi} with the over-all incident free-stream (translational) energy-transfer formula

$$\begin{aligned} C_{HFMi} &= \left(\frac{\gamma+1}{\gamma} \sqrt{\frac{2}{\gamma}} \frac{1}{4\sqrt{\pi}} \right) \frac{1}{M_o} \\ &= \frac{0.288}{M_o} \end{aligned}$$

*Personal communications from H. T. Nagamatsu.

for $\gamma = 1.4$. This yields

$$\left(\frac{C_H}{C_{HFMi}} \right)_{\max} = 1.24 \text{ at } M_o = 19.2$$

$$\left(\frac{C_H}{C_{HFMi}} \right)_{\max} = 1.76 \text{ at } M_o = 25.1$$

The theory would predict

$$\frac{C_H}{C_{HFMi}} = \left(\frac{C_{Hi} - C_{HW}}{C_{HFM}} \right)_{\max} - D^2 \left(1 - \frac{F}{C} \sqrt{\frac{\gamma-1}{2} \frac{T_w}{T_s}} \right)^2 \left(\frac{n_s}{n_e} \right)_{\max} (C, M_o) - \left(\frac{F}{C} \right)^2 \left(\frac{\gamma-1}{2} \frac{T_w}{T_s} \right) \quad (A-4)$$

where n_s/n_e is a weak function of the value of C and M_o .

Equation (A-4) provides one more relationship which, when solved simultaneously with Eqs. (A-1) through (A-3), can serve to define unambiguously the set of parameters C , D , F . However, it can be seen immediately from the low value of C_H/C_{HFMi} and from Fig. 8 that the solution of Eq. (A-4) will yield value of F too large to remain in the domain of validity of this cold-wall theory.

Concluding Remarks

In summary, the theoretical trends are found to be in accord with all the trends exhibited by the experimental data, both those relating to the induced pressure and those concerning the leading-edge heat transfer.

However, the comparison of data with theory, as well as the

inspection of the heat-transfer measurements, indicates that this series of tests involves a thermal-accommodation coefficient which is very low. Rough calculations show that convergence of all tests requires F of about 2.5; that is, a thermal-accommodation coefficient of about 40 per cent.

This is also an indication of strongly specular reflection. Consequently, the assumption of $\bar{\theta} = \pi/2$ made in the analysis should be revised.*

Apparently, in spite of the low wall temperature the wall-emission velocity, V_e , in the experiments of Ref. 1 was not sufficiently low to satisfy the conditions implied in the theory. Although it is possible to find a consistent set of empirical correlation parameters to fit the data and theory together, this is not meaningful until more tests properly planned as indicated by the theory become available.

*Note that the effect of $\bar{\theta}$ can be partly compensated for by choosing D properly. This is the reason that a better empirical correlation of the pressure data with $F = 1$ can be obtained than of the heat-transfer data.

REFERENCES

1. Nagamatsu, H. T., and R. E. Sheer, Jr., High Temperature Rarefied Ultra-High Mach Number Flow Over a Flat Plate, Reprint 1137-60, American Rocket Society Semi-Annual Meeting, Los Angeles, May 9-12, 1960.
2. Aroesty, J., Pressure Distributions on Flat Plates at Mach 4 and Low Density Flow, University of California Institute of Engineering Research Report HE-150-157, July, 1958.
3. Laurmann, J. A., "The Free Molecule Probe and Its Use for the Study of Leading Edge Flows," Phys. of Fluids, Vol. 1, No. 6, November-December, 1958, pp. 469-477.
4. Baker, R.M.L., Jr., and A. F. Charwat, "Transitional Correction to the Drag of a Sphere in Free-Molecule Flow," Phys. of Fluids, Vol. 1, No. 2, March-April, 1958, pp. 73-87.
5. Charwat, A. F., "Lift and Pitching Moment in Near-Free-Molecule Flow," in Symposium on Aerodynamics of the Upper Atmosphere, D. J. Masson, (comp.), The RAND Corporation, Report R-339, June 8-10, 1959.
6. Lees, L., A Kinetic Theory Description of Rarefied Gas Flows, Guggenheim Aeronautical Laboratory, California Institute of Technology, Memorandum No. 51, December, 1959.
7. Willis, D. R., "A Study of Near-Free-Molecule Flow," in Symposium on the Aerodynamics of the Upper Atmosphere, D. J. Masson, (comp.), The RAND Corporation, Report R-339, June 8-10, 1959.
8. Willis, D. R., A Study of Some Nearly Free Molecular Flow Problems, Princeton University Aeronautical Engineering Laboratory, Report No. 440, 1958.
9. Hurlbut, F. C., "Studies of Molecular Scattering at the Solid Surface," J. Appl. Phys., Vol. 28, No. 8, 1957, pp. 844-850.
10. Schamberg, R., A New Analytic Representation of Surface Interaction for Hyperthermal Free-Molecule Flow with Application to Neutral-Particle Drag Estimates of Satellites, The RAND Corporation, RM-2313, January 8, 1959.
11. Oguchi, Hakuro, "The Sharp Leading Edge Problem in Hypersonic Flow," 2nd International Symposium on Rarefied Gas Dynamics, Berkeley, California, August 3-6, 1960. (To be published, Academic Press.)
12. Liu, F. C., "Contributions to the Theory of Almost-Free-Molecule Flows," in Rarefied Gas Dynamics, F. N. Devienne, (ed.), Pergamon Press, London, 1960.